University of Alberta

Library Release Form

Name of Author: Yue Wu

Title of Thesis: Low-Complexity Detection for Multiple Antenna Wireless Communication Systems

Degree: Master of Science

Year this Degree Granted: 2007

Yue Wu
306-1102 Hermitage Rd
Edmonton, AB, T5A 4M3

Date: _____

University of Alberta

Low-Complexity Detection for Multiple Antenna Wireless Communication Systems

by

Yue Wu

A thesis submitted to the Faculty of Graduate Studies and Research in partial fulfillment of the requirements for the degree of **Master of Science**.

Department of Electrical and Computer Engineering

Edmonton, Alberta

Fall 2007

University of Alberta

Faculty of Graduate Studies and Research

The undersigned certify that they have read, and recommend to the Faculty of Graduate Studies and Research for acceptance, a thesis entitled **Low-Complexity Detection for Multiple Antenna Wireless Communication Systems** submitted by Yue Wu in partial fulfillment of the requirements for the degree of **Master of Science**.

Chintha Tellambura (Supervisor)

Dr. Bin Han (External)

Dr. Hai Jiang

Date: _____

Abstract

Multiple-input multiple-output (MIMO) wireless systems use antenna arrays at both the transmitter and receiver to achieve high spectral efficiency. Low-complexity detection is essential for the implementation of MIMO systems. In this thesis, a symbol detector for wireless systems using space division multiple access (SDMA) and orthogonal frequency division multiplexing (OFDM) is derived. The detector uses a sphere decoder (SD) and has much less computational complexity than the naive maximum likelihood (ML) detector in high SNR. Two new detectors for a hybrid system with the combination of spatial multiplexing (SM) and space-time block codes (STBC) are also derived. The new optimal detectors utilize the block structure of STBC and the SD. An optimal detector based on an ordering SD for MIMO OFDM systems by taking advantage of the high correlation among neighboring subcarriers in the system is also derived.

The ML detection problem in MIMO systems is then relaxed and a family of constrained detectors is developed. Real constrained detectors and decision feedback detectors are proposed by forcing the relaxed solution to be real. Modulus constrained subgroup detectors are developed for both unitary and non-unitary constellations. A new ordering scheme using these constrained detectors is proposed to achieve a trade-off between interference suppression and noise enhancement. Moreover, to mitigate the error propagation inherent in decision feedback detectors, a combined constrained and decision feedback detector is introduced. These constrained detectors are sub-optimal but they have much less complexity than the SD based optimal detectors in low SNR.

Acknowledgements

I could not have completed this work without the generous support of many people.

First and foremost, I am deeply indebted to my supervisor, Prof. Chintha Tellambura, for his valuable guidance, encouragement, patience, and financial support throughout the course of my study. Prof. Tellambura's knowledge, insight, and work ethic are an inspiration to me. I consider myself extremely privileged for having him as my supervisor.

I would also like to thank Dr. Bin Han and Dr. Hai Jiang for taking the time to serve on my committee.

I had the privilege of working with many talented people. I am grateful to Tao Cui, Luqing Wang, Yu Fu, Dung Ngoc Dao, Alireza Ghaderipoor, Mahdi Hajiaghayi, Zhongshan Zhang, Xinwei Deng, Wei Zhang, Yunxia Chen, and many others in our lab, for their helpful advice.

My thanks also go to Bo Hu, Xiaodi Zhang, Zhengang Chen, Xiaofeng Liang, Keith Goertzen, Cody Thiessen, Kenny Moreau, Karen Ridgway, Joy Davis, Rachael Tyler, Glen David Dickie, and Stephanie Dickie. Their friendship has made my Canadian experience an enjoyable and memorable one.

Finally, I owe my gratitude to my parents for their unconditional love and support.

Table of Contents

List of Tables

List of Figures

List of Acronyms

Acronyms	**Definition**
AWGN	Additive white Gaussian noise
BER	Bit error rate
BPSK	Binary phase shift keying
CDMA	Code Division Multiple Access
CLS	Constrained least squares
CP	Cyclic prefix
CSI	Channel state information
DFD	Decision feedback detector
DFT	Discrete Fourier Transform
GMMSE	Generalized minimum mean squared error
LS	Least squares
MIMO	Multiple-input and multiple-output
ML	Maximum likelihood
MMSE	Minimum mean squared error
MSE	Mean squared error
OFDM	Orthogonal Frequency Division Multiplexing
PAM	Pulse amplitude modulation
PSK	Phase shift keying
QAM	Quadrature amplitude modulation
QPSK	Quadrature phase shift keying

SINR	Signal-to-interference and noise ratio
SNR	Signal-to-noise ratio
SD	Sphere Decoder
STBC	Space-time block codes
V-BLAST	Vertical Bell Laboratories Layered Space-Time Architecture
ZF	Zero forcing

List of Notations

$(\cdot)^*$	Complex conjugation of the argument
$(\cdot)^T$	Transpose of the argument
$(\cdot)^H$	Conjugate transpose of the argument
$(\cdot)^\dagger$	Moore-Penrose pseudo-inverse of the argument
$\mathrm{Re}\{\cdot\}$	Real part of the argument
$\mathrm{Im}\{\cdot\}$	Imaginary part of the argument
$\mathrm{E}\{\cdot\}$	Expectation of the argument
$\|(\cdot)\|^2$	2-norm of the argument
$\mathbb{Z}$	The set of integers
$\mathbb{R}$	The set of real numbers
$\mathbb{C}$	The set of complex numbers
$\mathbb{C}^K$	The set of all complex $K \times 1$ vectors
$\mathbf{A}$	The Matrix $\mathbf{A}$
$\mathbf{a}$	The vector $\mathbf{a}$
$\mathrm{Tr}(\mathbf{M})$	The trace of the matrix $\mathbf{M}$
$\mathcal{CN}(\mu, \sigma^2)$	A complex Gaussian random variable (RV) with mean μ and variance σ^2
$\mathbf{I}_N$	The $N \times N$ identity matrix
$\mathrm{diag}(\mathbf{a})$	The diagonal matrix formed by vector $\mathbf{a}$
$\delta_{i,j}$	The Kronecker delta $\delta_{i,j} = 1$ if $i = j$ and $\delta_{i,j} = 0$ if $i \neq j$ where $i, j \in \mathbb{Z}$
(n, m)	A MIMO system with n transmit antennas and m receive antennas

Chapter 1

Introduction

1.1 Background and Motivation

Wireless communications has experienced an explosive growth in the past few decades. The 3rd generation (3G) and beyond 3rd generation wireless systems will provide mobile and stationary users with wireless multimedia services such as video conference, high speed internet access, and mobile computing [1]. The rapidly rising demand for these high data-rate services along with high mobility and high quality services are driving the recent developments in wireless technologies and inspiring many for broadband wireless applications. Research developments at the physical layer regarding efficient coding and modulation schemes and signal processing techniques to improve the quality and spectral efficiency of wireless communications are crucially important.

1.2 Multiple Input Multiple Output (MIMO) Systems

Since the wireless radio spectrum is limited, much research focuses on spectrally efficient transmission. The use of multiple antennas at transmitter and receiver,

popularly known as multiple input multiple output (MIMO), is an emerging cost-effective technology that offers substantial improvements in spectral efficiency [2]. Teletar [3] and Foschini and Gans [4] show that there is a large capacity (i.e., date rate) gain of MIMO systems; i.e., the capacity (data rate) grows at least linearly with the number of transmit antennas, provided that the number of receive antennas is greater than or equal to the number of transmit antennas. To realize this potential capacity, many MIMO schemes have been proposed, which can be classified into two major categories: 1) capacity-oriented techniques such as layered space-time processing [5]; 2) quality-oriented techniques such as space-time coding (STC) [6–9]. Space-time refers to the fact that coding is performed across both spatial and temporal domains.

1.3 Space-Time Coding (STC)

Space-time coding (STC) [6–9] has recently emerged as one of the most active research areas in wireless communications. STC systems process the transmit and receive signal waveforms in temporal, spatial and coding dimensions to deliver high data rates with diversity and coding gains. STC has been adopted in the 3G cellular standards such as WCDMA and cdma2000, and has also been proposed for many other wireless systems such as local-loop applications [10] and wide area packet data access [11].

STC can be divided into space-time trellis coding and space-time block coding. In space-time trellis coding [6], all data are trellis encoded across the transmit antennas and standard maximum likelihood decoding techniques are used at the receiver. Therefore, the full diversity order and substantial coding gains, can be achieved. The disadvantage of this approach is that the decoding complexity increases exponentially with the transmission rate. Hence it is not practical to employ space-time trellis codes with a large number of transmit antennas or when a high spectral efficiency is required.

Space-time block coding (STBC) [7–9] provides low decoding complexity while retaining acceptable performance. It provides a simple way to upgrade current wire-

less systems to MIMO systems while keeping a full diversity gain. It, however, is not designed to provide significant coding gains.

1.4 Spatial Multiplexing

One simple approach that takes advantage of the capacity of the MIMO system is spatial multiplexing (SM) [12]. SM divides the input data stream into multiple substreams to be sent over multiple transmit antennas. The receiver processes all the spatial streams to recover the original data. Linear receivers, such as zero-forcing (ZF) or minimum mean squared error (MMSE), and non-linear receivers, such as V-BLAST [13], provide low-complexity suboptimal data detection. Unfortunately, these receivers incur a significant performance loss compared to the maximum likelihood (ML) receiver.

1.5 Space Division Multiple Access

To increase the wireless system capacity and improve the spectral efficiency, multiple access techniques are required in resource critical wireless applications. The use of SM for multiple access is called space division multiple access (SDMA). SDMA typically employs an antenna array and allows different users to share the same spectrum [14–18]. This sharing is achieved by exploiting differences in geographical positions of the users and steering a directional beam toward each user while cancelling out any interference. In [14], a scheme based on direction-of-arrival (DOA) estimation is proposed to separate signals from different users. In many applications, so-called wideband SDMA separates different users based on their channel transfer function vectors, often referred to as their spatial signatures. Reference [15] exploits the finite alphabet property of digital signals to simultaneously estimate the users' array response vectors and the symbol sequence for each signal. In [17], a recursive estimation algorithm is developed to recover multiple signals from intersymbol interference (ISI)

and co-channel interference (CCI) by taking advantage of a special structure of the array output and the finite-alphabet property of digital signals.

1.6 Orthogonal Frequency Division Multiplexing

Conventional modulation schemes are limited in their maximum data rate in multipath channels due to the ISI caused by the multipath dispersion. Without equalization, the lower limit on symbol period is given by the channel delay spread. To achieve higher data rates, complex equalization is required at the receiver.

Orthogonal frequency division multiplexing (OFDM) [19–21] uses the Fast Fourier Transform (FFT) to multiplex the data on orthogonal subcarriers. This significantly increases symbol period on each subcarrier, which effectively mitigates the influence of multipath fading. OFDM thus converts a frequency selective channel into a number of parallel flat-fading channels, each of which can be easily equalized.

1.7 Thesis Contributions

Existing sub-optimal detectors for MIMO systems incur a performance loss compared with the ML detector. However, the brute-force ML detector is not deemed practical due to its high complexity. Therefore it is of interest to develop optimal detectors with low-complexity compared to the brute-force ML detectors. In Chapter 2, a new detector based on the sphere decoder for OFDM/SDMA based wireless systems is proposed. The use of sphere decoder achieves optimal detection with computational complexity much less than the naive ML detector in high SNR. Furthermore, we show how the CLS detector of [22] can be used to detect non-unitary signals. A hybrid orthogonal STBC and SM system is also considered. Such hybrid systems that provide a trade off between the rate and the diversity gain are of interest, but their optimal detectors have not yet been reported. Two new optimal detectors for these hybrid systems are proposed. Our algorithms can also be viewed as a generalization of the

conventional SD to handle matrix symbols. Finally, a new low complexity optimal detector is proposed for a fast fading MIMO OFDM system by taking advantage of the high correlation among neighboring subcarriers. In the proposed algorithm, the subcarriers are partitioned into a number of groups such that the correlation among the subcarriers in each group is high. Within each group, a symbol-detection reordering is performed on the center subcarrier and the SD operates on that order. The same ordering is then used on other subcarriers in the group.

Although these detectors has low complexity in high SNR, their worst-case complexity is exponential in the number of transmit antennas, and their average complexity is high in low SNR or for large systems [23]. Both performance and complexity gaps between the ML detector and the existing sub-optimal detectors have motivated the development of alternative detectors. In Chapter 3, the ML MIMO detection problem is relaxed to develop a family of constrained detectors. Real constrained detectors and decision feedback detectors are proposed for real constellations by forcing the relaxed solution to be real. Modulus constrained subgroup detectors are developed as MIMO detectors for both unitary and non-unitary constellations. A new ordering scheme using these constrained detectors is proposed to achieve a tradeoff between interference suppression and noise enhancement. Moreover, to mitigate the error propagation inherent in decision feedback detectors, a combined constrained and decision feedback detector is introduced. These constrained detectors are suboptimal but they have much less complexity than the SD based optimal detectors in low SNR.

Chapter 4 concludes the thesis and outlines future work in this area.

Chapter 2

Low-Complexity Optimal Detection for MIMO Systems

This chapter presents several low-complexity optimal MIMO detectors. In Section 2.1, a symbol detector is derived for wireless systems using space division multiple access (SDMA) and orthogonal frequency division multiplexing (OFDM). This detector uses a sphere decoder (SD) and has much less computational complexity than the naive maximum likelihood (ML) detector. In Section 2.2, two new detectors are derived for a hybrid system with the combination of spatial multiplexing (SM) and space-time block codes (STBC). The new detectors utilize the block structure of STBC and the SD. Optimal detection is performed with computational complexity much less than the brute-force ML search. In Section 2.3, a detector based on symbol detection reorder and SD is derived for MIMO OFDM systems by exploiting the high correlation among neighboring subcarriers.

2.1 Low-Complexity Optimal Detection for SDMA Systems

The combination of SDMA and OFDM for wireless networks exploits the advantages of both [22, 24, 25]. For example, in the uplink, the base station handles the SDMA function while the user terminals are plain OFDM modems. This asymmetry keeps the overall system cost low. However, previously-developled minimum mean squared error (MMSE) detectors [24] perform worse than the ML detector. The detector designed in [22] is specifically for unitary signals and outperforms the MMSE detector. A minimum bit error rate multiuser detector is designed in [26]. Reference [27] develops two linear demodulators for minimizing the probability of error. However, all these approaches incur a significant performance loss compared with the ML detector.

A new detector based on a sphere decoder (SD) is proposed for OFDM/SDMA based wireless systems. Sphere decoding [28] has been investigated for multiple antenna systems in [29]. The sphere decoder (SD) [28, 30], proposed in the context of the closest point searches in lattices, efficiently implements the ML detector. SD provides the same error performance as the brute-force ML detector. The use of the SD is further investigated in [31, 32]. The complexity of SD depends critically on the ordering of the columns of the channel matrix.The average complexity of the sphere decoding used for ML detection in flat fading multiple-antenna systems is polynomial (often sub-cubic) for a wide range of signal-to-noise ratios (SNRs). With the use of sphere decoding, optimal detection becomes feasible with computational complexity much less than the naive ML detector. Furthermore, the CLS detector of [22] is extended to detect non-unitary signals.

2.1.1 System Model

The uplink of an OFDM/SDMA system (Fig. 2.1) with U users and a basestation (BS) is considered. Each user transmit with a single antenna and the BS has $A \geq 1$

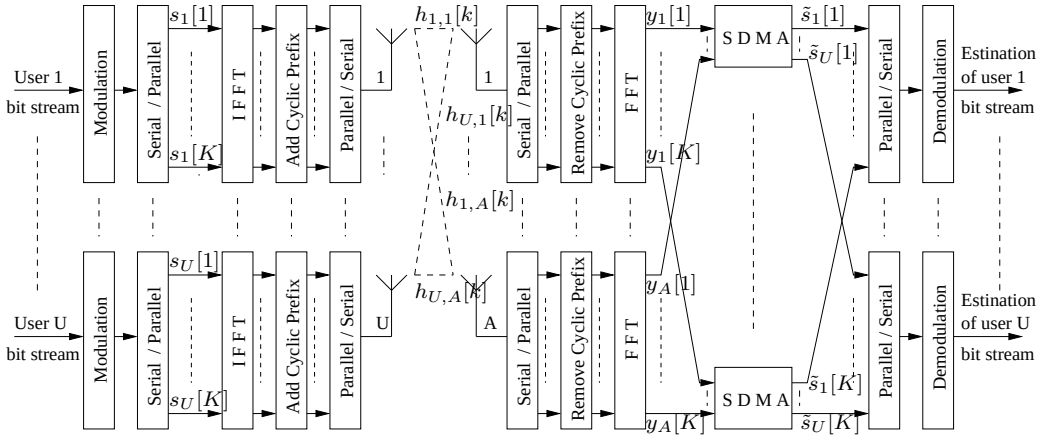

Fig. 2.1. System model.

receive antennas. The number of simultaneous users is no greater than the number of BS antennas. The bit stream of user u is modulated and a block of K modulated symbols is converted to a serial stream of $s_u[1], \cdots, s_u[K]$. This frequency domain series is fed into a K-tap inverse fast Fourier transform (IFFT) to obtain time-domain samples. A cyclic prefix and the samples are transmitted through a multipath fading channel. The cyclic prefix is removed at the receiver. The cyclic prefix is longer than the channel delay spread. The received signals at BS antenna a are converted to a parallel stream. A K-tap fast Fourier transform (FFT) operator is used to obtain $y_a[1], \cdots, y_a[K]$, which are processed by SDMA algorithms to separate different users and provide the estimated data $\tilde{s}_u[1], \cdots, \tilde{s}_u[K]$ as for user u.

After the removal of the cyclic prefix, the k-th subcarrier output is given by

$$\mathbf{y} = \mathbf{H}\mathbf{s} + \mathbf{n}, \tag{2.1}$$

where $\mathbf{y} = [y_1[k], \cdots, y_A[k]]^T$ is the received signals, $\mathbf{s} = [s_1[k], \cdots, s_U[k]]^T$ is the transmitted signals from U users, $\mathbf{n} = [n_1[k], \cdots, n_A[k]]^T$ is the additive white Gaussian noise, and

$$\mathbf{H} = \begin{bmatrix} h_{1,1}[k] & \cdots & h_{U,1}[k] \\ \vdots & \ddots & \vdots \\ h_{1,A}[k] & \cdots & h_{U,A}[k] \end{bmatrix} \tag{2.2}$$

is the frequency domain channel transfer function matrix, where $h_{a,u}[k]$ is the channel

between the u-th user and the a-th BS antenna. Assume $h_{a,u}[k]$ are uncorrelated, time-invariant, and complex Gaussian distributed fading processes with zero mean and unit variance. Since SDMA processing is applied on a per-carrier basis, symbol detection can also be solved per subcarrier. For notational simplicity, the index $[k]$ is dropped.

2.1.2 New Detector

Given the signal model (2.1), the optimal receiver must find the signal vector nearest to the received vector $\mathbf{y}$. Thus, the ML detector is given by

$$\tilde{\mathbf{s}} = \arg \min_{\mathbf{s} \in \mathcal{Q}^U} \|\mathbf{y} - \mathbf{H}\mathbf{s}\|^2, \tag{2.3}$$

where $\mathbf{y} \in \mathcal{R}^A$, $\mathbf{H} \in \mathcal{R}^{A \times U}$ and $\mathcal{Q} = \{-(2P-1), \cdots, 2P+1\}$ is a Pulse Amplitude Modulation (PAM) constellation of P elements. Since any quadrature amplitude modulation (QAM) constellation can be decoupled into real part and image part and transformed into real PAM constellations, this formulation (2.3) is valid for QAM too. The case of M-ary phase shift keying (M-PSK) is also treated later. A brute force ML algorithm must search all P^U possible values of $\mathbf{s}$. Hence, its complexity is exponential in U (the number of unknown variables).

The original SD by Fincke and Phost [28] restricts the search space to the candidate signals within a hypersphere of an initial radius. Whenever a valid candidate is found, the radius may be updated. Eq. (2.3) is equivalent to

$$\begin{aligned} \tilde{\mathbf{s}} &= \arg \min_{\mathbf{s} \in \mathcal{Q}^U} (\mathbf{H}^\dagger \mathbf{y} - \mathbf{s})^H \mathbf{R}^H \mathbf{R} (\mathbf{H}^\dagger \mathbf{y} - \mathbf{s}) \\ &= \arg \min_{\mathbf{s} \in \mathcal{Q}^U} (\mathbf{s} - \hat{\mathbf{s}})^H \mathbf{R}^H \mathbf{R} (\mathbf{s} - \hat{\mathbf{s}}) \end{aligned} \tag{2.4}$$

where $\hat{\mathbf{s}} = \mathbf{H}^\dagger \mathbf{y}$ and $\mathbf{R}$ is an upper triangular matrix such that $\mathbf{R}^H \mathbf{R} = \mathbf{H}^H \mathbf{H}$. Let the entries of $\mathbf{R}$ be denoted by r_{ij}, $i \leq j$. Since the number of users U is always less than or equal to the number of BS antennas A, $\mathbf{H}^H \mathbf{H}$ has full rank (positive definite). The diagonal terms of $\mathbf{R}$ are non-zero ($r_{ii} \neq 0$). A candidate is inside a hypersphere

of radius r when

$$(\mathbf{s}-\hat{\mathbf{s}})^H\mathbf{R}^H\mathbf{R}(\mathbf{s}-\hat{\mathbf{s}}) = \sum_{i=1}^{U} r_{ii}^2 \left\|s_i-\rho_i\right\|^2 \le r^2 \tag{2.5}$$

where $\rho_i = \hat{s}_i - \sum_{j=i+1}^{U} \frac{r_{ij}}{r_{ii}}(s_j-\hat{s}_j)$. The initial radius r is assumed to be large enough so that the hypersphere (2.5) contains at least one candidate solution. The initial radius may be chosen according to the noise variance [29].

Since each term in (2.5) is nonnegative, the partial sums must also be less than r^2. This fact can be used to derive a set of admissible values for s_u $(u = U, U-1, \ldots, 1)$ as

$$\mathcal{L}_u = \left\{ t \,\middle|\, \lceil \rho_u - r_u/r_{uu} \rceil \le t \le \lfloor \rho_u + r_u/r_{uu} \rfloor, t \in \mathcal{Q} \right\} \tag{2.6}$$

where $r_u^2 = r^2 - \sum_{i=u+1}^{U} r_{ii}^2 \|s_i-\rho_i\|^2$, $s_i \in \mathcal{L}_i$, $\lceil x \rceil$ is the smallest integer greater than or equal to x and $\lfloor x \rfloor$ is the largest integer less than or equal to x. In (2.6), the signal constellation $\mathcal{Q}$ can be either PAM or QAM (expressed as two real PAM constellations). Eq. (2.6) generates all signal vectors satisfying (2.5), the number of which is much smaller than $|\mathcal{Q}|^U$.

If $\mathcal{Q}$ is M-PSK, (2.6) is not directly applicable ($\mathcal{Q}$ is generally not decomposable into two real PAM constellations). The set of lists for $u = U, U-1, \ldots, 1$ is formed as

$$\mathcal{L}_u = \left\{ t \,\middle|\, r_{uu}^2 \left\|t-\rho_i\right\|^2 \le r_u^2, t \in \mathcal{Q} \right\}. \tag{2.7}$$

Once all the candidate signal vectors are generated via (6) or (7), the ML estimate is given by the candidate vector which minimizes (4). Putting all these ideas together, we propose the following new detector algorithm:

1 Input ($\mathbf{y}$, $\mathbf{H}$, r, $\mathcal{Q}$);

2 $[\mathbf{Q}, \mathbf{R}] = qr(\mathbf{H})$; $\hat{\mathbf{s}} = \mathbf{H}^{\dagger}\mathbf{y}$; $i = U$; $l = 1$; $\rho_U = \hat{s}_U$; $d^2 = r^2$;$r_U^2 = r^2$; $\mathcal{L}_U = \emptyset$; found=0;

3 Generate $\mathcal{L}_i$ using (6) or (7);

4 If $\mathcal{L}_i \neq \emptyset$ and $i = 1$, goto 8;

5 If $\mathcal{L}_i \neq \emptyset$, $\rho_{i-1} = \hat{s}_{i-1} - \sum_{j=i}^{U} \frac{r_{i-1,j}}{r_{i-1,i-1}}(s_j - \hat{s}_j)$, $r_{i-1}^2 = r_i^2 - r_{ii}^2 \|s_i - \rho_i\|^2$, $i = i - 1$, $l = 1$, goto 3;

6 If $i = U$, if found=1, go to 9, else increase r, $l = 1$, goto 3;

7 $i = i + 1$, $l = l + 1$, if $l > M$, goto 4, else goto 3;

8 found=1, $\mathbf{s}^* = \mathbf{s}$, $\tilde{d}^2 = r_1^2 - r_{11}^2 \|s_1 - \rho_1\|^2$, $l = 1$, goto 3;

9 If $\tilde{d}^2 < d^2$, $d = \tilde{d}$, goto 7, else return $\mathbf{s}^*$.

2.1.3 Non-unitary Signals

An M-QAM vector can be represented as a weighted sum of $N/2$ QPSK vectors when $M = 2^N$ and N is an even number [33]. That is, for $z \in M$-QAM and $z_i \in$QPSK, $0 \leq i < N/2$, the M-QAM symbol can be represented as

$$z = \sum_{i=0}^{N/2-1} 2^i \left(\frac{\sqrt{2}}{2}\right) z_i. \tag{2.8}$$

For example, 16QAM transmit vector $\mathbf{s}$ can be written as $\mathbf{s} = \sqrt{2}\mathbf{s}_1 + \frac{\sqrt{2}}{2}\mathbf{s}_2$ where $\mathbf{s}_1$ and $\mathbf{s}_2$ are QPSK vectors. Thus (2.1) becomes

$$\mathbf{y} = \begin{pmatrix} \sqrt{2}\mathbf{H} & \frac{\sqrt{2}}{2}\mathbf{H} \end{pmatrix} \begin{pmatrix} \mathbf{s}_1 \\ \mathbf{s}_2 \end{pmatrix} + \mathbf{n}. \tag{2.9}$$

Therefore a 16QAM system with U users and A receive antennas is equivalent to a QPSK system with $2U$ users and A receive antennas. Similarly, any other M-QAM system can also be expressed as an equivalent QPSK system.

However, the CLS detector in [22] may not be applied directly when $2U \geq A$. one of the conditions of the CLS detector in [22] is that the number of users is less than that of receive antennas. If this condition is not met, a rank deficiency arises from the singular value decomposition of the channel matrix. This limitation translates into

the condition of $2U \leq A$ for non-unitary signals. To solve this problem, a modified CLS detector is proposed for the rank-deficient channel matrix.

Since $\mathbf{s}$ is a vector of constant modulus signals, solving (2.3) is equivalent to solving

$$\begin{aligned}\tilde{\mathbf{s}} &= \arg\min_{\mathbf{s}\in\mathcal{Q}^U} \|\mathbf{y}-\mathbf{H}\mathbf{s}\|^2 + \sigma_n^2\|\mathbf{s}\|^2 \\ &= \arg\min_{\mathbf{s}\in\mathcal{Q}^U} \{\mathbf{s}^H(\mathbf{H}^H\mathbf{H}+\sigma_n^2\mathbf{I})\mathbf{s} - \mathbf{y}^H\mathbf{H}\mathbf{s} - \mathbf{s}^H\mathbf{H}^H\mathbf{y}\} \\ &= \arg\min_{\mathbf{s}\in\mathcal{Q}^U} \{\mathbf{s}^H\mathbf{H}_{eq}^H\mathbf{H}_{eq}\mathbf{s} - \mathbf{y}_{eq}^H\mathbf{H}_{eq}\mathbf{s} - \mathbf{s}^H\mathbf{H}_{eq}^H\mathbf{y}_{eq}\}, \end{aligned} \tag{2.10}$$

where σ_n^2 is the variance of Guassian noise, $\mathbf{H}_{eq}$ is from the Cholesky factorization $(\mathbf{H}^H\mathbf{H}+\sigma_n^2\mathbf{I}) = \mathbf{H}_{eq}^H\mathbf{H}_{eq}$, and $\mathbf{y}_{eq} = (\mathbf{H}_{eq}^H)^{-1}\mathbf{H}^H\mathbf{y}$. $\mathbf{H}_{eq}$ becomes the equivalent channel matrix while $\mathbf{y}_{eq}$ is the equivalent received signal vector. This solves the rank-deficient problem when $2U \geq A$. Therefore the modified CLS detector can be used with M-QAM.

2.1.4 Simulation Results

A current wireless local-area network (LAN) standard at 5GHz is ETSI BRAN HIPERLAN/2 [34]. Such a wireless LAN with four simultaneously transmitting users and a BS with four antennas is considered here. The simulation parameters are summarized in Table 2.1.

TABLE 2.1

Simulation Parameters.

Parameter	Value
Number of simultaneous users	4
Number of basestation antennas	4
Bandwidth for each user (MHz)	20
Number of subcarriers	64
Number of data subcarriers	48
Cyclic Prefix Length	16

The error performance of six detectors (SB is the sensitive bits algorithm from [35]) for QPSK (Fig. 2.2) and 16QAM (Fig. 2.3) is compared. In low SNR, the MMSE detector gains 2 dB over the V-BLAST detector [13], but the latter outperforms the former by more than 2 dB in high SNR. The MMSE detector performs slightly better than the CLS detector for both QPSK and 16QAM. The ZF detector performs the worst in all SNR, and our new detector performs significantly better than the other five detectors. It gains about 7 dB over the V-BLAST detector at a BER of 10^{-2}. This gain increases as the SNR increases. The diversity order (the magnitude of the slope of the error rate curve) is higher for our new detector than that for V-BLAST.

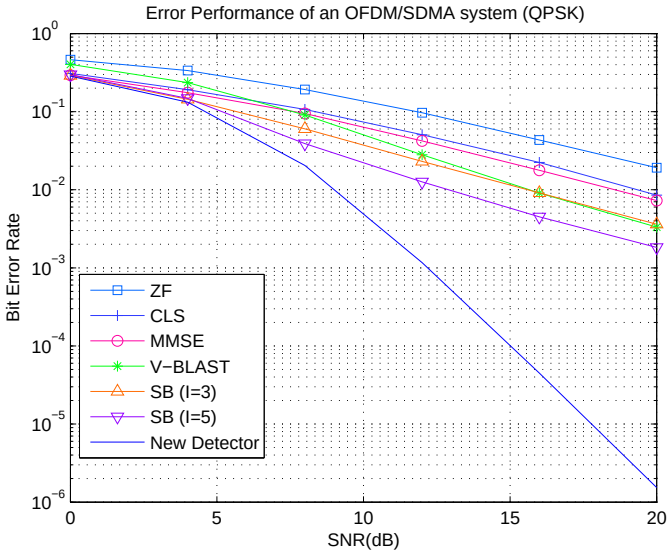

Fig. 2.2. Bit error rate of the detectors for QPSK.

Fig. 2.4 shows the performance of the six detectors for the coded system. QPSK modulation and the industry-standard generator polynomials $g_1 = 133_{OCT}$ and $g_2 = 171_{OCT}$ of rate 1/2 convolutional code with constraint length 7 are used. As before, our new detector performs significantly better than the other detectors.

Fig. 2.5 shows the computational complexity of the six detectors for QPSK. The complexity of the new detector is high for low SNR (two orders of magnitude higher) but decreases significantly as SNR increases, approaching that of the V-BLAST detector.

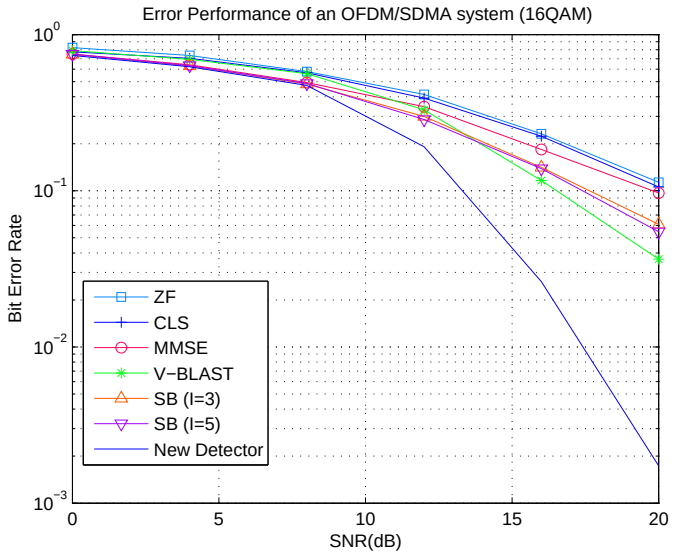

Fig. 2.3. Bit error rate of the detectors for 16QAM.

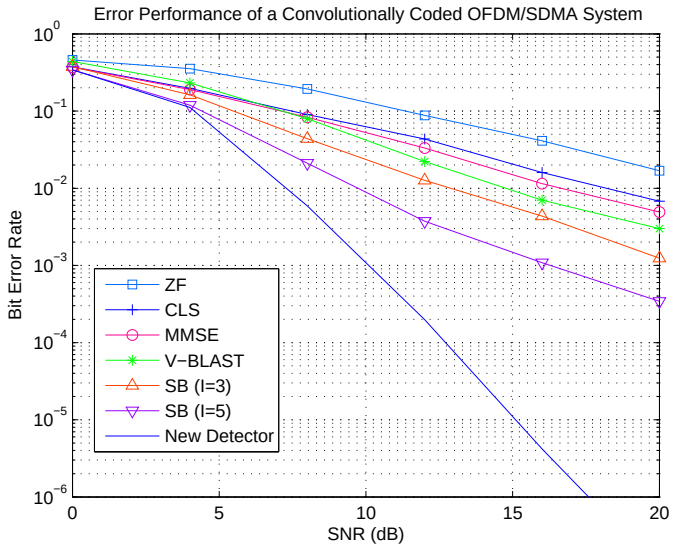

Fig. 2.4. Bit error rate with convolutional coding.

2.2 Low-Complexity Optimal Detection for Hybrid STBC and SM

The idea of combining orthogonal space-time block codes (STBCs) and spatial multiplexing (SM) was originally proposed in [36]. SM can transmit at a rate of n symbols

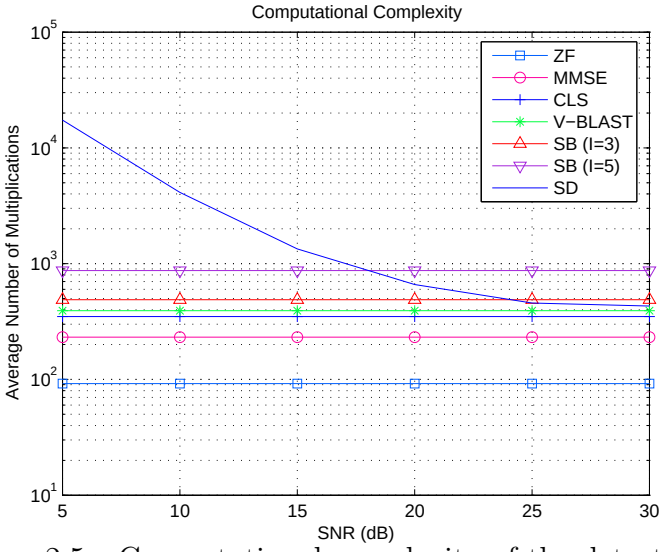

Fig. 2.5. Computational complexity of the detectors.

per time slot for a system with n transmit antennas and m receive antennas ($m \leq n$), but does not achieve the maximum diversity order of nm of this system. On the other hand, orthogonal STBCs can transmit only up to a rate of 1 symbol per time slot regardless of the number of transmit antennas, but achieve the maximum diversity order of nm. Thus, such hybrid systems that provide a trade off between rate and the diversity gain are of interest, but their optimal detectors have not yet been reported.

Some suboptimal detectors, namely the ZF group detector, the MMSE group detector, and the QR group successive interference cancelation (SIC) detector, have been proposed in [37, 38] for the STBC/SM hybrid system. All these detectors incur a significant performance loss compared to the ML detector. In this section, two new optimal detectors are proposed for the orthogonal STBC/SM hybrid systems. Our algorithms can also be viewed as a generalization of the conventional SD to handle input matrix symbols. The simulation results show that the new detectors achieve the ML performance with low complexity for a wide range of SNRs.

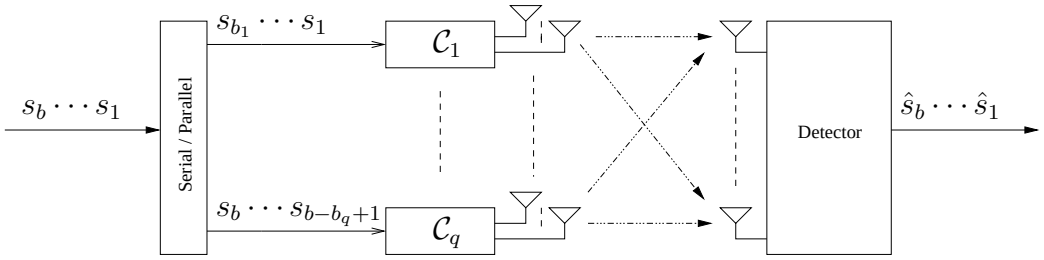

Fig. 2.6. System model.

2.2.1 System Model

The STBC/SM hybrid system consists of a serial/parallel converter, a number of STBC encoders, and a detector. The input data stream $s_1 \cdots s_b$ is split into q groups of length $b_1, \cdots, b_q$ with $b_1 + \cdots + b_q = b$. The q groups are sent into q independent STBC encoders, $\mathcal{C}_1, \cdots, \mathcal{C}_q$, respectively. Each STBC encoder has $n_i (1 \leq i \leq q)$ transmit antennas with $n_1 + \cdots + n_q = n$. All the STBC encoded symbols are transmitted simultaneously from n transmit antennas. The i-th group of data stream is encoded by $\mathcal{C}_i$ and transmitted from n_i antennas in t_i time slots. In this section, we assume $t_1 = \cdots = t_q = t$. With m receive antennas at the receiver, the detector provides the estimates $\hat{s}_b \cdots \hat{s}_1$. The system model is shown in Fig. 2.6.

The received signal over t time slots is given by

$$\mathbf{y} = \mathbf{H}\mathbf{s} + \mathbf{n}, \tag{2.11}$$

where $\mathbf{H} = [h_{kl}]$ is the $m \times n$ channel matrix with $h_{kl} \sim \mathcal{CN}(0, 1)$ for $k = 1, \cdots, m$ and $l = 1, \cdots, n$ and $\mathrm{E}\{h_{kl} h^*_{k'l'}\} = \delta_{k,k'} \delta_{l,l'}$, $\mathbf{s}$ is the $n \times t$ matrix after STBC encoding, and $\mathbf{n}$ is the $m \times t$ matrix of additive white noise $\mathcal{CN}(0, \sigma_n^2)$ terms. $\mathbf{H}$ is assumed constant over a block of t time slots but changes independently from block to block. The transmit signal matrix $\mathbf{s}$ can be written as $\mathbf{s} = [\mathbf{s}_1^T \ \mathbf{s}_2^T \ \cdots \ \mathbf{s}_q^T]^T$, where $\mathbf{s}_i$ is the coded block from the i-th STBC encoder. The detector operates with the full channel state information.

2.2.2 Detection of the STBC/SM hybrid system

The detectors proposed in [38] consist of two parts. The first part is a group receiver that separates each STBC block from one another. The second part consists of a number of STBC decoders. Unlike these detectors that separate the group detector and STBC decoder, our new SD-based detectors exploits the block structure due to the STBC.

2.2.2.1 MMSE group detector

The i-th MMSE group detector [38] for the signals transmitted from $\mathcal{C}_i$ is given by

$$\begin{aligned}\mathbf{W}_i &= \arg \min_{W} \ \mathrm{E}(||\mathbf{W}\mathbf{y} - \mathbf{H}_i\mathbf{s}_i||^2) \\ &= \mathbf{H}_i\mathbf{H}_i^H(\mathbf{H}\mathbf{H}^H + \sigma_n^2\mathbf{I}_m)^{-1}, 1 \leq i \leq q. \end{aligned} \tag{2.12}$$

With the corresponding virtual channel matrix $\mathbf{H}_i$, the output of the i-th MMSE group detector is processed by an STBC decoder to obtain the estimation of $s_{b_1+\cdots+b_{i-1}+1}$, $\cdots$, $s_{b_1+\cdots+b_i}$.

2.2.2.2 ZF group detector

ZF group detectors for $(3,3)$ and $(4,4)$ hybrid systems with Alamouti codes [7] are proposed in [39]. Here a ZF group detector is proposed for an $(8,8)$ hybrid system with the Alamouti code.

The 8×8 channel matrix decomposed into four 4×4 matrices is given by

$$\mathbf{H} = \begin{bmatrix} \mathbf{A}_4 & \mathbf{B}_4 \\ \mathbf{C}_4 & \mathbf{D}_4 \end{bmatrix}, \tag{2.13}$$

where $\mathbf{A}_4, \mathbf{B}_4, \mathbf{C}_4$, and $\mathbf{D}_4$ are all 4×4 matrices. The ZF group detector at this level is

$$\mathbf{W}_4 = \begin{bmatrix} \mathbf{B}_4^{-1} & -\mathbf{D}_4^{-1} \\ \mathbf{A}_4^{-1} & -\mathbf{C}_4^{-1} \end{bmatrix}. \tag{2.14}$$

Thus

$$\mathbf{W}_4\mathbf{H} = \begin{bmatrix} \mathbf{B}_4^{-1}\mathbf{A}_4 - \mathbf{D}_4^{-1}\mathbf{C}_4 & \mathbf{0}_4 \\ \mathbf{0}_4 & \mathbf{A}_4^{-1}\mathbf{B}_4 - \mathbf{C}_4^{-1}\mathbf{D}_4 \end{bmatrix} \tag{2.15}$$

and the output of this detector is $\tilde{\mathbf{y}} = \mathbf{W}_4\mathbf{H}\mathbf{s}$, which can be written as

$$\begin{bmatrix} \tilde{\mathbf{y}}_1 \\ \tilde{\mathbf{y}}_2 \end{bmatrix} = (\mathbf{B}_4^{-1}\mathbf{A}_4 - \mathbf{D}_4^{-1}\mathbf{C}_4) \begin{bmatrix} \mathbf{s}_1 \\ \mathbf{s}_2 \end{bmatrix} \tag{2.16}$$

$$\begin{bmatrix} \tilde{\mathbf{y}}_3 \\ \tilde{\mathbf{y}}_4 \end{bmatrix} = (\mathbf{A}_4^{-1}\mathbf{B}_4 - \mathbf{C}_4^{-1}\mathbf{D}_4) \begin{bmatrix} \mathbf{s}_3 \\ \mathbf{s}_4 \end{bmatrix} \tag{2.17}$$

For (2.16), the equivalent channel matrix $\mathbf{H}_{eq}$ can be written as

$$\mathbf{H}_{eq} = (\mathbf{B}_4^{-1}\mathbf{A}_4 - \mathbf{D}_4^{-1}\mathbf{C}_4) = \begin{bmatrix} \mathbf{A}_2 & \mathbf{B}_2 \\ \mathbf{C}_2 & \mathbf{D}_2 \end{bmatrix}, \tag{2.18}$$

where $\mathbf{A}_2, \mathbf{B}_2, \mathbf{C}_2$, and $\mathbf{D}_2$ are all 2×2 matrices. The ZF group detector at this level is

$$\mathbf{W}_2 = \begin{bmatrix} \mathbf{B}_2^{-1} & -\mathbf{D}_2^{-1} \\ \mathbf{A}_2^{-1} & -\mathbf{C}_2^{-1} \end{bmatrix}. \tag{2.19}$$

Thus

$$\mathbf{W}_2\mathbf{H}_{eq} = \begin{bmatrix} \mathbf{B}_2^{-1}\mathbf{A}_2 - \mathbf{D}_2^{-1}\mathbf{C}_2 & \mathbf{0}_2 \\ \mathbf{0}_2 & \mathbf{A}_2^{-1}\mathbf{B}_2 - \mathbf{C}_2^{-1}\mathbf{D}_2 \end{bmatrix} \tag{2.20}$$

and the output of this detector is $\hat{\mathbf{y}} = \mathbf{W}_2\mathbf{H}_{eq}\mathbf{s}$, which can be written as

$$\hat{\mathbf{y}}_1 = (\mathbf{B}_2^{-1}\mathbf{A}_2 - \mathbf{D}_2^{-1}\mathbf{C}_2)\mathbf{s}_1 \tag{2.21}$$

$$\hat{\mathbf{y}}_2 = (\mathbf{A}_2^{-1}\mathbf{B}_2 - \mathbf{C}_2^{-1}\mathbf{D}_2)\mathbf{s}_2. \tag{2.22}$$

With the corresponding virtual channel matrix $(\mathbf{B}_2^{-1}\mathbf{A}_2 - \mathbf{D}_2^{-1}\mathbf{C}_2)$, $\hat{\mathbf{y}}_1$ is processed by an STBC decoder to estimate s_1 and s_2. The detection for $s_3, \cdots, s_8$ is similar. This method can also be extended to any system provided the number of antennas is $2^k, k = 2, 3, \cdots$.

2.2.2.3 New detector A

The ML detector for the signal model in (2.11) is given by

$$\tilde{\mathbf{s}} = \arg \min_{\mathbf{s} \in \mathcal{Q}^n} \|\mathbf{y} - \mathbf{H}\mathbf{s}\|^2. \tag{2.23}$$

Let the QR decomposition of $\mathbf{H}$ be $\mathbf{H} = \mathbf{Q}\mathbf{R}$, where $\mathbf{Q}$ is a unitary matrix and $\mathbf{R}$ is an upper triangular matrix. Let $\hat{\mathbf{y}} = \mathbf{Q}^H\mathbf{y}$. Thus, Eq. (2.11) is equivalent to $\hat{\mathbf{y}} = \mathbf{R}\mathbf{s} + \hat{\mathbf{n}}$, where $\hat{\mathbf{n}} = \mathbf{Q}^H\mathbf{n}$. $\mathbf{R}$ is an upper triangle matrix given by

$$\mathbf{R} = \begin{bmatrix} \mathbf{R}_{11} & \mathbf{R}_{12} & \cdots & \mathbf{R}_{1,q} \\ \mathbf{0} & \mathbf{R}_{22} & \cdots & \mathbf{R}_{2,q} \\ \vdots & \vdots & \ddots & \vdots \\ \mathbf{0} & \mathbf{0} & \cdots & \mathbf{R}_{q,q} \end{bmatrix}. \tag{2.24}$$

The k-th component of block $\hat{\mathbf{y}}$ can be written as

$$\hat{\mathbf{y}}_k = \mathbf{R}_{k,k}\mathbf{s}_k + \sum_{i=k+1}^{q} \mathbf{R}_{k,i}\mathbf{s}_i + \hat{\mathbf{n}}_k. \tag{2.25}$$

Thus (2.23) is equivalent to

$$\tilde{\mathbf{s}} = \arg \min_{\mathbf{s} \in \mathcal{Q}^n} \underbrace{\sum_{k=1}^{q} \|\hat{\mathbf{y}}_k - \mathbf{R}_{k,k}\mathbf{s}_k - \sum_{i=k+1}^{q} \mathbf{R}_{k,i}\mathbf{s}_i\|^2}_{f(\mathbf{s})}. \tag{2.26}$$

The key complexity-reducing idea of SD is to generate only admissible signal points such that

$$f(\mathbf{s}) \leq r^2. \tag{2.27}$$

The initial radius r may be chosen according to the noise variance [30] and can be increased if it is too small to contain any admissible solution. The problem is that $f(\mathbf{s})$ is expressed in terms of matrix symbols $\mathbf{s}_k$, but the admissible signal points should be based upon the constellation symbols s_k ($k = 1, \ldots, b$). To overcome this

problem, we use the linear dispersion representation: the matrix symbol $\mathbf{s}_k$ can then be written in terms of the underlying constellation symbols as

$$\mathbf{s}_k = \sum_{s_n \in G_k} (\mathrm{Re}\{s_n\}\mathbf{A}_n + \sqrt{-1}\mathrm{Im}\{s_n\}\mathbf{B}_n), \tag{2.28}$$

where $s_n \in G_k$ are the constellation symbols encoded in $\mathbf{s}_k$ and $\mathbf{A}_n, \mathbf{B}_n$ are fixed basis matrices of $\mathcal{C}_k$ and they satisfy certain orthogonality conditions [40]. As shown in [40], the q-th term in (2.26) can be written as

$$\begin{aligned} &\|\mathbf{R}_{q,q}\|^2 \sum_{s_n \in G_q} \|s_n - 1/\|\mathbf{R}_{q,q}\|^2 \\ &\times (\mathrm{ReTr}\{\hat{\mathbf{y}}_q \mathbf{R}_{q,q}\mathbf{A}_n\} - i\mathrm{ImTr}\{\hat{\mathbf{y}}_q \mathbf{R}_{q,q}\mathbf{B}_n\})\|^2. \end{aligned} \tag{2.29}$$

Now a looser condition than (6) is that the term (2.29) should be less than r^2. Using this slightly loose condition, the admissible set of $s_n \in G_q$ can be obtained. In fact, assume $s_1^q, \cdots, s_{b_q}^q$ are the independent symbols in the set of $s_n \in G_q$. Since each term in (2.29) is nonnegative, a necessary condition for $\mathbf{s}$ to lie inside the hypersphere is that

$$\begin{aligned} &\|\mathbf{R}_{q,q}\|^2 \|s_1^q - 1/\|\mathbf{R}_{q,q}\|^2 \\ &\times (\mathrm{ReTr}\{\hat{\mathbf{y}}_q \mathbf{R}_{q,q}\mathbf{A}_1^q\} - i\mathrm{ImTr}\{\hat{\mathbf{y}}_q \mathbf{R}_{q,q}\mathbf{B}_1^q\})\|^2 \le r^2. \end{aligned} \tag{2.30}$$

Once an s_1^q that satisfies the condition of (2.30) is chosen, a new radius $r_{q,1}^2$ is derived accordingly after the deduction of the contribution of s_1^q in (2.29) from r^2. The next step is to choose an s_2^q satisfying the new radius. If there is no such s_2^q, the previous step must be retraced to obtain a new s_1^q and therefore a new $r_{q,1}^2$. This same process continues until it reaches $s_{b_1}^1$, obtaining an admissible set of $s_n \in G_q$ satisfying (2.27). The radius r is then updated and the search space is limited by the new radius. The above process repeats for the $q-1$-th term to obtain the admissible set of $s_n \in G_{q-1}$. This process repeats until all admissible $s_n \in G_k$ $(k = 1, \ldots, q)$ are generated. Of course, the admissible vectors are generated in depth-first fashion and whenever an admissible vector is found the radius r is updated and the search space is limited by the new radius. The above process continues until the ML solution is found.

2.2.2.4 New detector B

An alternative detector we propose here is that the structure of STBC is processed before a conventional SD is used to achieve ML detection.

Without the loss of generality, the STBC encoders are assumed to be the Alamouti code [7]. Since the $\mathbf{s}$ in (2.11) is an $n \times 2$ matrix, a conventional SD can not be employed directly with (2.11). In fact, (2.11) can be written as

$$\begin{bmatrix} y_{11} & y_{12} \\ \vdots & \vdots \\ y_{m,1} & y_{m,2} \end{bmatrix} = \begin{bmatrix} h_{11} & \cdots & h_{1,n} \\ \vdots & \ddots & \vdots \\ h_{m,1} & \cdots & h_{m,n} \end{bmatrix} \begin{bmatrix} s_1 & -s_2^* \\ s_2 & s_1^* \\ \vdots & \vdots \\ s_{n-1} & -s_n^* \\ s_n & s_{n-1}^* \end{bmatrix} + \mathbf{n}. \tag{2.31}$$

Taking advantage of the orthogonal structure of the STBC, (2.31) can be transformed to

$$\mathbf{y}' = \mathbf{H}'\mathbf{s}' + \mathbf{n}', \tag{2.32}$$

where $\mathbf{y}' = \begin{bmatrix} y_{11} & y_{12}^* & \cdots & y_{m,1} & y_{m,2}^* \end{bmatrix}^T$, $\mathbf{s}' = \begin{bmatrix} s_1 & s_2 & \cdots & s_{n-1} & s_n \end{bmatrix}^T$, and

$$\mathbf{H}' = \begin{bmatrix} h_{11} & h_{12} & \cdots & h_{1,n-1} & h_{1,n} \\ h_{12}^* & -h_{11}^* & \cdots & h_{1,n}^* & -h_{1,n-1}^* \\ \vdots & \vdots & \ddots & \vdots & \vdots \\ h_{m,1} & h_{m,2} & \cdots & h_{m,n-1} & h_{m,n} \\ h_{m,2}^* & -h_{m,1}^* & \cdots & h_{m,n}^* & -h_{m,n-1}^* \end{bmatrix}. \tag{2.33}$$

Thus $\mathbf{s}'$, the part that contains $\mathbf{s}$, has become a vector in (2.32), which means the conventional SD can now be applied to obtain the ML estimate of $\mathbf{s}'$.

The ML detector for (2.32) is given by

$$\tilde{\mathbf{s}}' = \arg \min_{\mathbf{s}' \in \mathcal{Q}^n} \|\mathbf{y}' - \mathbf{H}'\mathbf{s}'\|^2. \tag{2.34}$$

Consider QAM for $\mathbf{s}'$. Since a QAM constellation can be decoupled into two real PAM constellations, solving (2.34) is equivalent to solving

$$\tilde{\mathbf{s}}'' = \arg \min_{\mathbf{s}'' \in \mathcal{Q}^{2n}} \|\mathbf{y}'' - \mathbf{H}''\mathbf{s}''\|^2, \tag{2.35}$$

where $\mathbf{y}'' = [\mathrm{Re}\{\mathbf{y}'\}^T \;\; \mathrm{Im}\{\mathbf{y}'\}^T]^T$, $\mathbf{s}'' = [\mathrm{Re}\{\mathbf{s}'\}^T \;\; \mathrm{Im}\{\mathbf{s}'\}^T]^T$, and

$$\mathbf{H}'' = \begin{bmatrix} \mathrm{Re}\{\mathbf{H}'\} & -\mathrm{Im}\{\mathbf{H}'\} \\ \mathrm{Im}\{\mathbf{H}'\} & \mathrm{Re}\{\mathbf{H}'\} \end{bmatrix}. \tag{2.36}$$

Eq. (2.35) can be written as

$$\begin{aligned} \tilde{\mathbf{s}}'' &= \arg \min_{\mathbf{s}'' \in \mathcal{Q}^{2n}} (\mathbf{H}''^{\dagger}\mathbf{y}'' - \mathbf{s}'')^H \mathbf{R}^H \mathbf{R} (\mathbf{H}''^{\dagger}\mathbf{y}'' - \mathbf{s}'') \\ &= \arg \min_{\mathbf{s}'' \in \mathcal{Q}^{2n}} (\mathbf{s}'' - \hat{\mathbf{s}}'')^H \mathbf{R}^H \mathbf{R} (\mathbf{s}'' - \hat{\mathbf{s}}''), \end{aligned} \tag{2.37}$$

where $\hat{\mathbf{s}}'' = \mathbf{H}''^{\dagger}\mathbf{y}''$ and $\mathbf{R}$ is an upper triangular matrix such that $\mathbf{R}^H\mathbf{R} = \mathbf{H}''^H\mathbf{H}''$. Let the entries of $\mathbf{R}$ be denoted by r_{ij}, $i \leq j$. In this section, we assume $m \geq n$ and the diagonal terms of $\mathbf{R}$ are non-zero ($r_{ii} \neq 0$). A candidate solution is inside the hypersphere of radius r when

$$(\mathbf{s}'' - \hat{\mathbf{s}}'')^H \mathbf{R}^H \mathbf{R} (\mathbf{s}'' - \hat{\mathbf{s}}'') = \sum_{i=1}^{2n} r_{ii}^2 \left\| s_i'' - \rho_i \right\|^2 \leq r^2, \tag{2.38}$$

where $\rho_i = \hat{s}_i'' - \sum_{j=i+1}^{2n} \frac{r_{ij}}{r_{ii}} (s_j'' - \hat{s}_j'')$. The initial radius may be chosen according to the noise variance [29]. The initial radius can be increased if it is too small to contain any candidate solution. Since each term in 2.38 is nonnegative, a necessary condition for $\mathbf{s}''$ to lie inside the hypersphere is that $r_{2n,2n}^2 \left\| s_{2n}'' - \hat{s}_{2n}'' \right\|^2 \leq r^2$, or equivalently

$$\left\lceil \hat{s}_{2n}'' - \frac{r}{r_{2n,2n}} \right\rceil \leq s_{2n}'' \leq \left\lfloor \hat{s}_{2n}'' + \frac{r}{r_{2n,2n}} \right\rfloor, \tag{2.39}$$

where $\lceil \cdot \rceil$ denotes the smallest integer greater than or equal to its argument. $\lfloor \cdot \rfloor$ denotes the largest integer less than or equal to its argument. The same process continues for s_{2n-1} and so on until it reaches s_1, obtaining a vector point satisfying (2.37). The radius r is then updated and the search space is limited by the new radius. The above process continues until no further points are found within the hypersphere. This process yields the ML solution.

For other orthogonal STBCs, $\mathbf{s}$ can always be transformed into a vector because of the orthogonality. For example, for an (n,m) hybrid system with a rate 3/4 STBC [40],

(2.11) can be written as

$$\begin{bmatrix} y_{11} & \cdots & y_{14} \\ \vdots & \ddots & \vdots \\ y_{m,1} & \cdots & y_{m,4} \end{bmatrix} = \begin{bmatrix} h_{11} & \cdots & h_{1,n} \\ \vdots & \ddots & \vdots \\ h_{m,1} & \cdots & h_{m,n} \end{bmatrix} \begin{bmatrix} s_1 & 0 & s_2 & -s_3 \\ 0 & s_1 & s_3^* & s_2^* \\ -s_2^* & -s_3 & s_1^* & 0 \\ \vdots & \vdots & \vdots & \vdots \\ s_{n-2} & 0 & s_{n-1} & -s_n \\ 0 & s_{n-2} & s_n^* & s_{n-1}^* \\ -s_{n-1}^* & -s_n & s_{n-2}^* & 0 \end{bmatrix} + \mathbf{n}. \tag{2.40}$$

Exploiting the orthogonal structure of the STBC, (2.40) can be transformed into

$$\mathbf{y}' = \mathbf{H}'\mathbf{s}' + \mathbf{n}', \tag{2.41}$$

where $\mathbf{y}' = \begin{bmatrix} y_{11} & y_{12} & y_{13}^* & y_{14} & \cdots & y_{m,1} & y_{m,2} & y_{m,3}^* & y_{m,4} \end{bmatrix}^T$,
$\mathbf{s}' = \begin{bmatrix} s_1 & s_2^* & s_3 & \cdots & s_{n-2} & s_{n-1}^* & s_n \end{bmatrix}^T$, and

$$\mathbf{H}' = \begin{bmatrix} h_{11} & -h_{13} & 0 & \cdots & h_{1,n-2} & -h_{1,n} & 0 \\ h_{12} & 0 & -h_{13} & \cdots & h_{1,n-1} & 0 & -h_{1,n} \\ h_{13}^* & h_{11}^* & h_{12}^* & \cdots & h_{1,n}^* & h_{1,n-2}^* & h_{1,n-1}^* \\ 0 & h_{12} & -h_{11} & \cdots & 0 & h_{1,n-1} & -h_{1,n-2} \\ \vdots & \vdots & \ddots & \vdots & \vdots & & \\ h_{m,1} & -h_{m,3} & 0 & \cdots & h_{m,n-2} & -h_{m,n} & 0 \\ h_{m,2} & 0 & -h_{m,3} & \cdots & h_{m,n-1} & 0 & -h_{m,n} \\ h_{m,3}^* & h_{m,1}^* & h_{m,2}^* & \cdots & h_{m,n}^* & h_{m,n-2}^* & h_{m,n-1}^* \\ 0 & h_{m,2} & -h_{m,1} & \cdots & 0 & h_{m,n-1} & -h_{m,n-2} \end{bmatrix}. \tag{2.42}$$

Thus $\mathbf{s}'$, the part that contains $\mathbf{s}$, has become a vector in (2.41), which means the conventional SD can now be applied to obtain the ML estimate of $\mathbf{s}'$.

2.2.3 Simulation Results

Fig. 2.7 (4QAM) and Fig. 2.8 (16QAM) show the error performance of an uncoded (4,4) STBC/SM hybrid system with two Alamouti encoders at the transmit side. The performance of a (2, 4) SM system (no STBC encoders) is included. Both these systems have the same date throughput. The ZF group/STBC detector performs the worst among all detectors. The MMSE group/STBC outperforms the ZF group/STBC by less than 2 dB for most of the SNR range. The QR group SIC/STBC detector has a 2 dB or more gain over the MMSE group/STBC one in high SNR. The new detector (either version A or B) outperforms the QR group SIC/STBC detector by more than 4 dB at the bit error rate (BER) of 10^{-4}. The MMSE detector for the equivalent SM system performs slightly better than the ZF group/STBC detector. The ML detector for the SM system performs worse than the MMSE/STBC detector in low SNR but outperforms the latter in high SNR.

For 16QAM, the performances of the ZF group/STBC detector and the MMSE detector for the SM system are very close. The MMSE group/STBC detector has a 2 dB gain over both of them in low SNR. In high SNR, the performance of the QR group SIC/STBC detector has about a 2 dB gain over the MMSE detector for the equivalent SM system. The new detector (either version A or B) significantly outperforms the QR group SIC/STBC detector by a 3 dB at a BER of 10^{-2}.

Fig. 2.9 shows the performance of the detectors in an uncoded (8,8) 4QAM STBC/SM hybrid system with 4 Alamouti encoders at the transmit side. The (4, 8) SM system has the same data throughput as the (8, 8) STBC/SM system. In high SNR, the MMSE group/STBC detector gains 6 dB over the ZF group/STBC, which has the worst performance among all. The QR group SIC/STBC detector outperforms the MMSE group/STBC one by more than 2 dB at the BER of 10^{-4}. The MMSE detector for the SM system outperforms the QR group SIC/STBC detector by 1 dB in high SNR. The ML detector for the SM system has a 3 dB gain over the MMSE detector for the same SM system. The new detector (either version A or B)

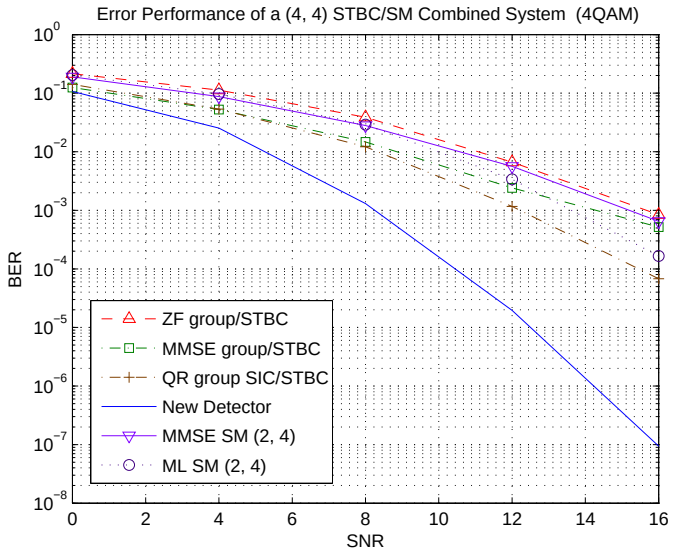

Fig. 2.7. Error Performance of a (4,4) STBC/SM system (4QAM).

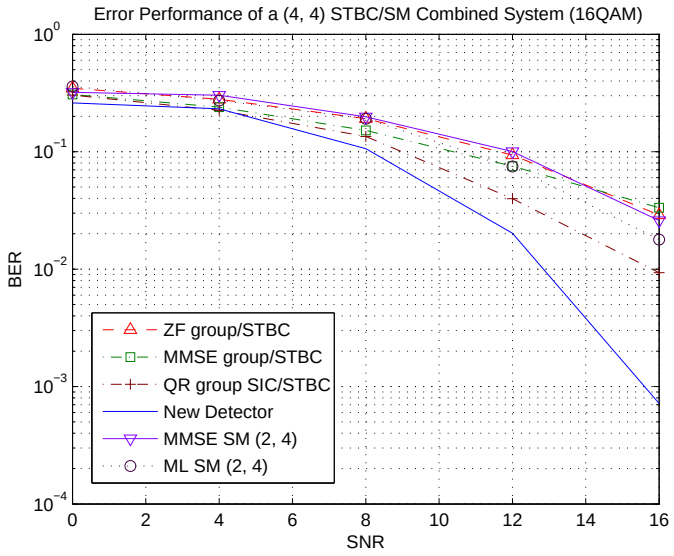

Fig. 2.8. Error Performance of a (4,4) STBC/SM system (16QAM).

outperforms the ML detector for the SM system by 4 dB and has the best performance among all.

Fig. 2.10 shows the computational complexity of a (4, 4) 4QAM STBC/SM hybrid system. The two new detectors have similar complexity. In low SNR, the new detectors have a high computational complexity, but the complexity decreases

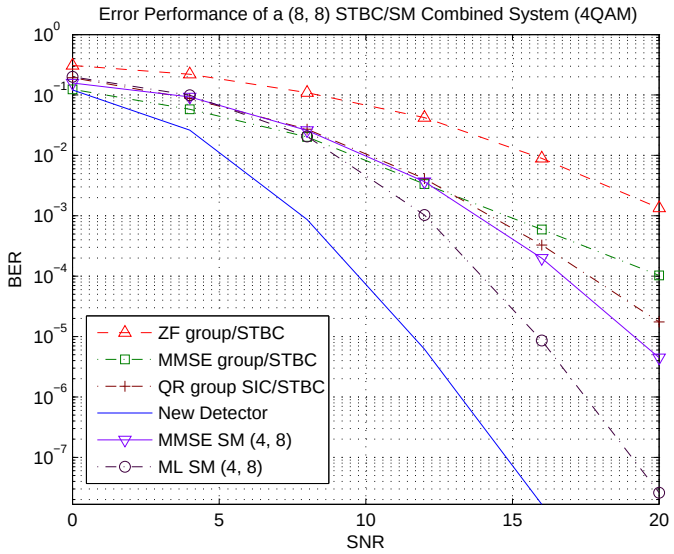

Fig. 2.9. Error Performance of a (8,8) STBC/SM system (4QAM).

significantly as the SNR increases. In high SNR, the complexity of the new detectors approaches that of the MMSE group/STBC detector. The complexity of both the detectors for the (2, 4) SM system is low as a result of the small number of transmit antennas. The complexity of the naive ML detector for the equivalent SM system increased exponentially with the increase of the number of transmit antennas.

2.3 Low-Complexity Optimal Detection for MIMO OFDM Systems

High data rate transmission in frequency selective fading channels can be achieved by the combination of the OFDM and the MIMO techniques. MIMO significantly increases the system capacity. For high data rate transmission, MIMO channels becomes frequency selective. Since OFDM converts a frequency selective fading channel into a set of flat fading channels, MIMO-OFDM transforms a frequency selective MIMO channel into a set of flat fading MIMO channels. A MIMO-OFDM system transmits independent OFDM modulated data from multiple antennas simultane-

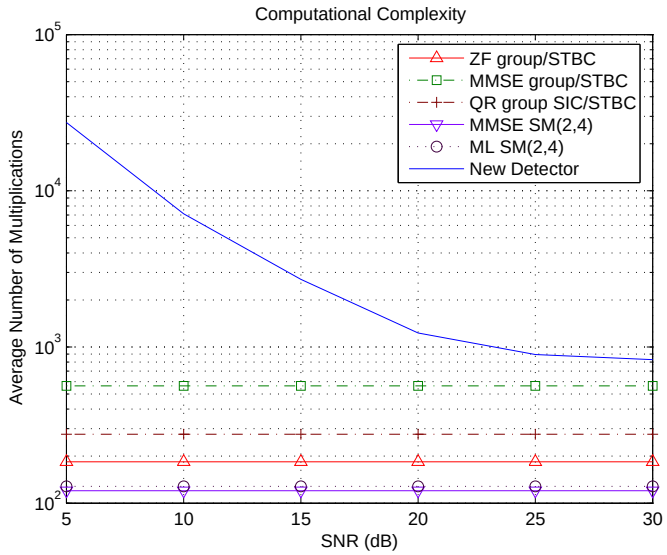

Fig. 2.10. Computational complexity of a (4,4) STBC/SM system (4QAM).

ously.

A V-BLAST detector for a MIMO OFDM system has been proposed in [41]. This detector utilizes the high correlation among neighboring subcarriers in some practical channel models. However, the V-BLAST detector incurs a significant performance loss over the ML detector. An SD with V-BLAST optimal detection ordering [29] is shown to reduce the complexity of the SD. However, depending on how often the ordering is performed, the complexity of the ordering itself may have a considerable impact on the overall complexity. In this section, a new low complexity optimal detector is proposed for a fast fading MIMO OFDM system by taking advantage of the high correlation among neighboring subcarriers in the system. In the proposed algorithm, the subcarriers are partitioned into a number of groups such that the correlation among the subcarriers in each group is high. Within each group, the symbol detection order is adjusted on the basis of the central subcarrier. The same order is then used on other subcarriers in the group. The simulation results shows that this new detector has a lower complexity than the conventional SD or the one in which the symbol-detection order is optimized for each subcarrier in the group, but it still achieves the ML performance.

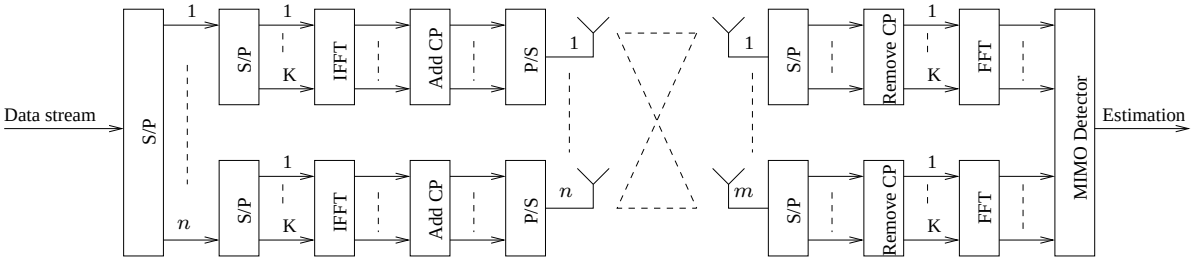

Fig. 2.11. System model.

2.3.1 System Model

Consider a MIMO OFDM system with n transmit antennas, m receive antennas, and K subcarriers. The date stream is converted into n parallel streams. Each of the parallel streams is again sent into a different serial/parallel converter, of which the output is fed into a K-tap inverse fast Fourier transform (IFFT). The output of the IFFT along with added cyclic prefix is converted into a serial stream and then transmitted through one of the n transmit antennas. The received signals at each of the m receive antennas are converted into parallel streams. After the cyclic prefix is removed, a K-tap FFT is performed and the output is fed into a MIMO detector. The system model is shown in Fig. 2.11.

Since each of the n streams undergoes the identical OFDM, each subcarrier is effectively an (n, m) narrow band MIMO system. MIMO detectors such as the SD can be used on each subcarrier. The channels between different transmit and receive antennas are statistically the same. The impulse response of one of the multipath channels can be written as $\mathbf{h} = [h_1, h_2, \cdots, h_L]^T$ where L is the number of multipath channel taps. The frequency response of the channel for an OFDM system with K subcarriers is given by $\mathbf{h}_{\mathcal{F}} = \mathbf{F}\mathbf{h}$, where $\mathbf{F}_{i,j} = (1/\sqrt{K})\exp(-j2\pi(((i-1)(j-1))/K)), i = 1, \cdots, K, j = 1, \cdots, L+1$. The correlation coefficient of subcarriers i and j can be written as

$$\rho_{i,j} = \frac{\mathbf{f}_i^H \mathrm{E}(\mathbf{h}\mathbf{h}^H)\mathbf{f}_j}{\sqrt{\mathbf{f}_i^H \mathrm{E}(\mathbf{h}\mathbf{h}^H)\mathbf{f}_i \mathbf{f}_j^H \mathrm{E}(\mathbf{h}\mathbf{h}^H)\mathbf{f}_j}}, \tag{2.43}$$

where $\mathbf{f}_k$ is the k-th column of $\mathbf{F}$.

2.3.2 New Detector

Since each subcarrier is effectively an (n, m) narrow band MIMO system, conventional MIMO detectors can be applied on each subcarrier. For example, ML detection is possible by using SD on each subcarrier. Although the SD has a much lower complexity than the brute-force ML detector, the overall complexity of using the SD on all subcarriers is high when the number of subcarriers is high.

The computational complexity of SD is sensitive to the ordering of the columns of the channel matrix [30]. Different ordering of the columns of channel matrix $\mathbf{H}$ can lead to a lower complexity than that of the unordered $\mathbf{H}$.

Let $r_{i,i}$ be the element of the upper triangular matrix from the QR decomposition of the channel matrix $\mathbf{H}$. Obviously, a larger $r_{i,i}$ corresponds to a smaller interval, which means less search for the i-th component and therefore reduces the complexity. By using the V-BLAST optimal detection ordering [42] to generate the permutation matrix Π, $\min_{1\leq i\leq n} r_{i,i}$ is maximized over all column permutations. Thus the maximum interval is minimized after the ordering and the search complexity is reduced. The column ordering $\Pi(n), \Pi(n-1), \cdots, \Pi(1)$ is recursively given by

$$\Pi(i) = \arg\max_{j\in\mathcal{I}_i}\{\mathbf{h}_i^T[\mathbf{I} - \mathbf{H}_{i,j}(\mathbf{H}_{i,j}^T\mathbf{H}_{i,j})^{-1}\mathbf{B}_{k,j}^T]\mathbf{h}_j\} \tag{2.44}$$

where $\mathbf{h}_i$ is the i-th column of $\mathbf{H}$, $\mathbf{H}_{i,j}$ is the $m \times (i-1)$ matrix formed by $\mathbf{h}_k$ with $k \in \mathcal{I}_i - \{j\}$.

Depending on how often the ordering is performed, the complexity of the ordering itself may have a considerable impact on the overall complexity. In a MIMO OFDM system with fast fading channels, performing ordering on all subcarriers is not desirable considering its impact on overall complexity.

In some practical channel models, such as non-line-of-sight (NLOS) HiperLAN/2 channel models A, B, C, and E, the correlation is high among neighboring subcarriers [41]. Taking advantage of the high correlation, the subcarriers are partitioned into a number of groups such that the correlation among subcarriers within each group is above a threshold value. Within each group, the V-BLAST column ordering is

performed on the center carrier before the conventional SD is applied. The same ordering is used on all other subcarriers in the group before the SD is performed on each of the subcarriers.

The following steps constitute the new detector algorithm:

1 Set the value of the threshold of the subcarrier correlation coefficient;

2 Partition the subcarriers into a number of groups of size k;

3 Perform the V-BLAST column permutation on the center carrier and apply SD after the ordering;

4 The column permutation matrix $\mathbf{\Pi}$ is recorded and applied to other subcarriers in the group;

5 SD is performed on these subcarriers after the ordering;

6 The same procedure is applied to other groups.

The ordering recorded from the center subcarrier in each group is not strictly optimal for other subcarriers in the group. However, due to the high correlations between the subcarriers within one group, the channels in the group change only slightly. Therefore it is reasonable to assume that the ordering of the center subcarrier is suboptimal for other subcarriers. The complexity is reduced to a lesser degree on the non-center subcarriers than it is on the center subcarrier.

2.3.3 Simulation Results

The ordered SD and the conventional SD are both ML. The error performance of the ordered SD is the same as that of a conventional SD without ordering. Without considering the complexity of the V-BLAST column permutation, the complexity of the ordered SD is related to the dimensions of the channel matrix. The higher the

dimensions are, the more complexity reduction the ordered SD provides. As the V-BLAST column permutation is performed only once for each group of subcarriers, the impact of the V-BLAST ordering to the overall complexity is negligible.

An OFDM system with 64 subcarriers and 16-tap cyclic prefix is simulated. The channel is non-line-of sight (NLOS) HiperLAN/2 channel models A [43] with root mean square (rms) delay spread of 50 ns. The maximum delay spread is 800 ns, which corresponds to 16 channel taps for a 20 MHz bandwidth sample spaced channel. Doppler spread is not considered here as the transmit and receive antennas are stationary. The threshold value is set to 0.8 and the number of subcarriers in each group is 8. Fig. 2.12 shows the error performance of a $(6, 6)$ MIMO OFDM system. The new detector has the same error performance as the conventional SD without ordering. The new detector significantly outperforms the V-BLAST detector. At the bit error rate of 10^{-2}, the new detector has a 6 dB gain over the V-BLAST detector. The new detector also has a larger diversity gain than the V-BLAST detector. Fig. 2.13 shows the complexity of a $(20, 20)$ MIMO OFDM system. The complexity is shown in the numbers of addition, multiplication, division, and square root. The solid lines are the complexity of the conventional SD detections on each subcarriers. The complexity of the new detector is shown in dotted line. The complexity reduction achieved by the new detector is larger in low SNR than in high SNR. Fig. 2.14 shows the complexity of a $(32, 32)$ MIMO OFDM system.

2.4 Summary

In this chapter, a symbol detector is derived for wireless systems using SDMA and OFDM. The detector uses a sphere decoder and has less computational complexity than the naive ML detector. Two new detectors are derived for a hybrid system with the combination of SM and STBC. They utilize the block structure of STBC and the SD. Optimal detection is performed with computational complexity less than the brute-force ML search. As well, a detector is derived based on an ordered SD

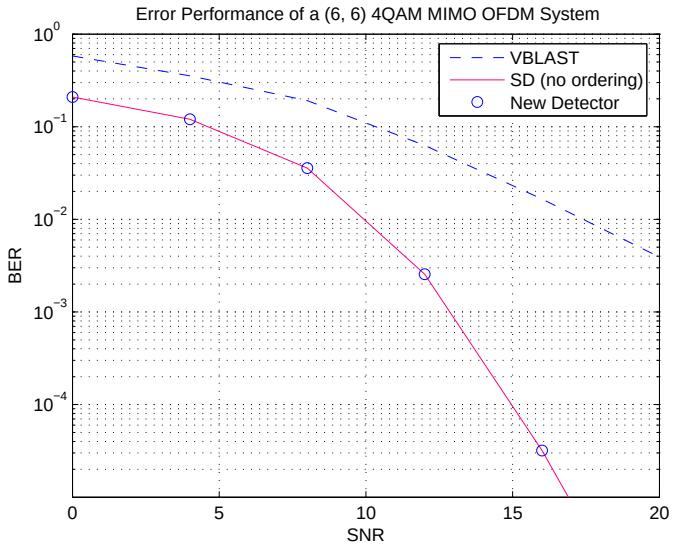

Fig. 2.12. Error Performance of a (6, 6) 4QAM MIMO OFDM System.

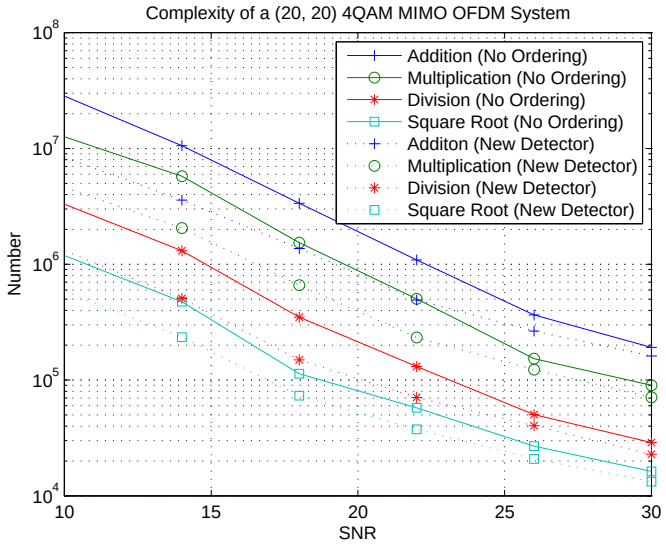

Fig. 2.13. Complexity of a (20, 20) 4QAM MIMO OFDM System.

for MIMO OFDM systems by exploiting of the high correlation among neighboring subcarriers. The simulation results show that these detectors are optimal and have significantly less complexity than the brute-force ML detector.

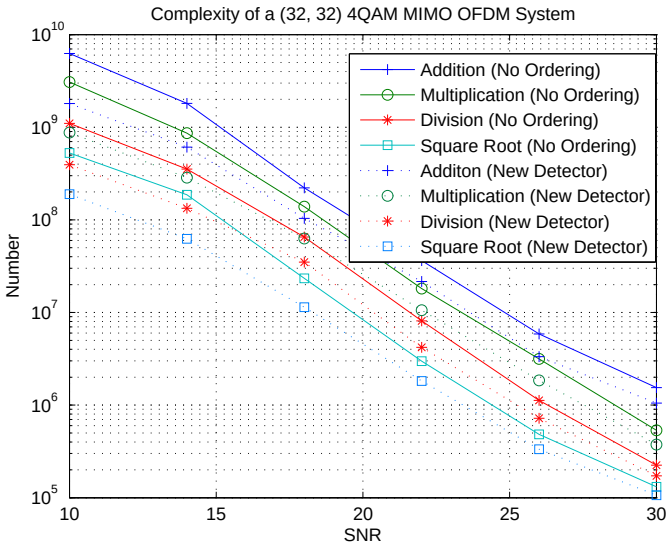

Fig. 2.14. Complexity of a (32, 32) 4QAM MIMO OFDM System.

Chapter 3

Constrained Detection for SM MIMO Systems

This chapter develops constrained detectors and constrained decision feedback detectors (DFDs) for SM MIMO systems. Section 3.1 introduces the background on this problem. In Section 3.2, real constrained and decision feedback detectors are proposed for real constellations by suppressing the imaginary interference component. The constrained least squares (CLS) detector of [22] is generalized by dividing the signal vector to several subgroups and applying the unitary constraints to these subgroups. Similarly, the generalized MMSE (GMMSE) detector [44] is extended to non-unitary constellations. In Section 3.3, a new ordering scheme that maximizes the signal-to-interference and noise ratio (SINR) at each step is proposed using the constrained detectors. Reference [45] shows that the first detected symbol limits the overall performance of V-BLAST. Thus the constrained detector and the DFD is combined to improve the quality of the first few detected symbols.

3.1 Introduction

3.1.1 Background

Various efficient signal detection algorithms for SM MIMO systems have been developed, among which the V-BLAST (vertical Bell Laboratories layered space time) detector [13] is a prime example. Although the optimal maximum likelihood detector (MLD) achieves the minimum error probability for independent and identically distributed (i.i.d.) random symbols, a requirement that holds in many cases, the complexity of the MLD grows exponentially with the number of transmit antennas and the number of bits that index each scalar constellation point, making it computationally prohibitive in most cases. Therefore, various computationally efficient suboptimal detectors such as the ZF detector and the MMSE detector have been developed. In [13], the V-BLAST detector with optimal ordering, nulling and interference cancellation is proposed. The equivalence between V-BLAST and a ZF decision feedback detector (DFD) is demonstrated [46]. If the nulling criterion is MMSE, the resulting MMSE-DFD [47] makes a trade-off between interference suppression and noise enhancement. However, these suboptimal detectors or equalizers perform much worse than the MLD. In [28, 29, 48], the sphere decoder (SD), offering optimal performance, is proposed as an MLD. Although it has low complexity in high SNR, its worst-case complexity is exponential in the number of transmit antennas, and its average complexity is high in low SNR or for large systems [23]. Both performance and complexity gaps between the MLD and the existing suboptimal detectors have motivated the development of alternative detectors.

The MIMO detection problem requires minimizing a quadratic cost function over the discrete set of all possible transmit vectors. In the relaxation approach, this discrete set is embedded in a larger bounded multidimensional continuous space and the minimization is performed over this continuous space subject to certain constraints. The resulting minimum solution is mapped back into the original discrete space. Several such constrained detectors have been developed [22, 44, 49–51]. For example,

a generalized MMSE (GMMSE) detector for code-division multiple-access (CDMA) systems is proposed [44], where the constrained optimization problem resulting from the relaxation of the BPSK vectors to be inside the unit hypersphere is solved via the convex duality theorem and gradient descent. In [22], a tighter relaxation is used in OFDM / SDMA systems employing unitary constellations by restricting the binary vectors on the hypersphere, resulting in the constrained least squares (CLS) detector. In [49], semidefinite relaxation (SDR) has been developed for BPSK-CDMA systems. SDR has also been extended to general M-PSK and quadrature amplitude modulation (QAM) constellations in [50, 52, 53].

3.1.2 System Model

Consider a standard MIMO system with n transmit antennas and m receive antennas. In SM, different antennas transmit independent signals rather than jointly encoded ones. That is, the input data stream is demultiplexed into n equal-rate substreams, and each of which is simultaneously sent through one of the n antennas over a rich scattering channel. Each receive antenna collects signals from all the n transmit antennas. A finite signal constellation $\mathcal{Q}$ is used. Consider a flat fading MIMO channel. The discrete-time equivalent baseband received signals can thus be written as

$$\mathbf{r} = \mathbf{H}\mathbf{x} + \mathbf{n}, \tag{3.1}$$

where $\mathbf{x} = [x_1, \ldots, x_n]^T$, $x_i \in \mathcal{Q}$ is the transmitted signal vector, $\mathbf{r} = [r_1, \ldots, r_m]^T$, $r_i \in \mathbb{C}$ is the received signal vector, $\mathbf{H} = [h_{i,j}] \in \mathbb{C}^{m \times n}$ is the channel matrix, and $\mathbf{n} = [n_1, \ldots, n_m]^T$, $n_i \in \mathbb{C}$ is an additive white Gaussian noise (AWGN) vector. The elements of $\mathbf{H}$ are i.i.d. complex Gaussian, $h_{i,j} \sim \mathcal{CN}(0, 1)$. The components of $\mathbf{n}$ are i.i.d. with $n_i \sim \mathcal{CN}(0, \sigma_n^2)$. The channel $\mathbf{H}$ is assumed known to the receiver and $n \leq m$. If $n > m$, the rank deficient problem can be transformed into a full rank problem as shown in [31]. Note (3.1) models any linear, synchronous and flat fading channels. Therefore, all our detectors can also be applied to CDMA systems.

Given the standard model (3.1), the MLD that minimizes the average error probability is

$$\hat{\mathbf{x}} = \arg\min_{\mathbf{x}\in\mathcal{Q}^n} \|\mathbf{r} - \mathbf{H}\mathbf{x}\|^2. \tag{3.2}$$

Due to the discrete nature of $\mathcal{Q}$, (3.2) is an NP-hard problem and exhaustive search for $\hat{\mathbf{x}}$ has a complexity exponential in n.

3.2 Constrained Detectors

3.2.1 Classic Linear Equalizers

We briefly review several classic linear equalizers. Since $\mathcal{Q} \subseteq \mathbb{C}$, a simple relaxation is to allow each $x_i \in \mathbb{C}$. This relaxation results in the well-known ZF linear equalizer and (3.2) becomes

$$\hat{\mathbf{x}}_{\text{ZF}} = D\left[\arg\min_{\mathbf{x}\in\mathbb{C}^n} \|\mathbf{r} - \mathbf{H}\mathbf{x}\|^2\right] \tag{3.3}$$

where $D[x]$ denotes the threshold detection rule that yields the constellation symbol closest to x. For a vector $\mathbf{x}$, $D[\mathbf{x}]$ operates on each element individually. The minimization part in (3.3) has the least squares (LS) solution and the ZF detector can be thus written as

$$\hat{\mathbf{x}}_{\text{ZF}} = D\left[\left(\mathbf{H}^H\mathbf{H}\right)^{-1}\mathbf{H}^H\mathbf{r}\right]. \tag{3.4}$$

If the same relaxation is combined with the minimization of the mean-square error between the transmitted signals and detected signals $E\{\|\mathbf{x} - \hat{\mathbf{x}}\|^2\}$, where the MMSE prefilter output is $\hat{\mathbf{x}} = \mathbf{G}\mathbf{r}$ ($\mathbf{G}$ is a prefilter matrix). Using the orthogonality principle [54], one can determine the optimal prefilter matrix and the MMSE linear equalizer is then given by

$$\hat{\mathbf{x}}_{\text{MMSE}} = D\left[\left(\mathbf{H}^H\mathbf{H} + \sigma_n^2\mathbf{I}_n\right)^{-1}\mathbf{H}^H\mathbf{r}\right]. \tag{3.5}$$

However, both the ZF and MMSE linear equalizers do not guarantee the optimal solution (2), due to the looseness of the relaxation.

For additional details, the reader is referred to [44, 55].

3.2.2 Real Constrained Equalizers

A real constellation $\mathcal{Q}$ has all real elements, e.g. binary phase shift keying (BPSK) and pulse amplitude modulation (PAM). If the real signals are transmitted through a complex channel as (3.1), the received signals are complex, and the ZF and MMSE solutions from (3.4) and (3.5) are usually complex vectors. However, the receiver has the *a prior* knowledge that the transmitted signals are real. Moreover, the imaginary part may cause additional interference. To impose a real constraint on (3.4) and (3.5), $\mathcal{Q}$ is relaxed to $\mathbb{R}$. Note that the complex system (3.1) can be transformed into a real system as

$$\tilde{\mathbf{r}} = \begin{bmatrix} \mathrm{Re}\{\mathbf{r}\} \\ \mathrm{Im}\{\mathbf{r}\} \end{bmatrix} = \begin{bmatrix} \mathrm{Re}\{\mathbf{H}\} \\ \mathrm{Im}\{\mathbf{H}\} \end{bmatrix} \mathbf{x} + \begin{bmatrix} \mathrm{Re}\{\mathbf{n}\} \\ \mathrm{Im}\{\mathbf{n}\} \end{bmatrix} = \tilde{\mathbf{H}}\mathbf{x} + \tilde{\mathbf{n}}. \tag{3.6}$$

The entries of $\tilde{\mathbf{n}}$ have zero means and variance $\sigma_n^2/2$. The ZF and MMSE linear equalizers for the equivalent real system (3.6) can be obtained as

$$\hat{\mathbf{x}}_{\mathrm{R-ZF}} = D\left[\left(\tilde{\mathbf{H}}^H\tilde{\mathbf{H}}\right)^{-1}\tilde{\mathbf{H}}^H\tilde{\mathbf{r}}\right] \tag{3.7}$$

and

$$\hat{\mathbf{x}}_{\mathrm{R-MMSE}} = D\left[\left(\tilde{\mathbf{H}}^H\tilde{\mathbf{H}} + \sigma_n^2/2\mathbf{I}_n\right)^{-1}\tilde{\mathbf{H}}^H\tilde{\mathbf{r}}\right] \tag{3.8}$$

where R-ZF and R-MMSE denote real constrained ZF and MMSE detectors. Since both $\tilde{\mathbf{H}}$ and $\tilde{\mathbf{r}}$ are real, $\hat{\mathbf{x}}_{\mathrm{R-ZF}}$ and $\hat{\mathbf{x}}_{\mathrm{R-MMSE}}$ are also real. Therefore, the real constraint is imposed implicitly.

Note that as the solution obtained by either (3.5) or (3.8) has a bias towards zero, the prefilter output $\hat{\mathbf{x}}$ should be scaled to maintain the average constellation power before applying threshold decision. By exploiting the power constraint or modulus constraint of each constellation, the performance of MMSE equalizers can be improved and $\hat{\mathbf{x}}$ needs not to be scaled.

3.2.3 Modulus Constrained Subgroup Detectors

When $\mathcal{Q}$ is complex, the modulus constraints of $\mathcal{Q}$ can be exploited. Consider a unitary constellation with unity modulus $|x_i|^2 = 1$, i.e., M-PSK. This pointwise constraint directly leads to the candidate vectors being on the hypersphere $\mathbf{x}^H\mathbf{x} = n$, e.g., the CLS [22]. However, to achieve better performance, tighter constraints are required. To this end, the vector $\mathbf{x}$ can be partitioned into $g > 1$ groups and each group is associated with a subvector $\mathbf{x}_i$ with size s_i, $i = 1, \ldots, g$, where $\sum_{i=1}^{g} s_i = n$. Each $\mathbf{x}_i$ can be relaxed on a s_i-dimensional hypersphere $\mathbf{x}_i^H\mathbf{x}_i = s_i$. The constrained detector is thus given by

$$\hat{\mathbf{x}}_{\text{CML}} = D\left[\underset{\mathbf{x}_1^H\mathbf{x}_1=s_1,\ldots,\mathbf{x}_g^H\mathbf{x}_g=s_g}{\arg\min} \|\mathbf{r}-\mathbf{H}\mathbf{x}\|^2\right] \tag{3.9}$$

where CML denotes constrained MLD[1]. The minimization problem in (3.9) can be written as

$$\begin{aligned} &\min_{\mathbf{x}} \|\mathbf{r}-\mathbf{H}\mathbf{x}\|^2 \\ &\text{s.t. } \mathbf{x}_1^H\mathbf{x}_1 = s_1, \ldots, \mathbf{x}_g^H\mathbf{x}_g = s_g. \end{aligned} \tag{3.10}$$

The Lagrangian $\mathcal{L}(\mathbf{x}, \lambda_1, \ldots, \lambda_g)$ for this minimization problem is

$$\mathcal{L}(\mathbf{x}, \lambda_1, \ldots, \lambda_g) = \|\mathbf{r}-\mathbf{H}\mathbf{x}\|^2 + \sum_{i=1}^{g} \lambda_i \left(\mathbf{x}_i^H\mathbf{x}_i - s_i\right). \tag{3.11}$$

Taking partial derivatives with respect to $\mathbf{x}$ the solution for $\mathbf{x}$ can be derived as

$$\hat{\mathbf{x}}(\lambda_1, \ldots, \lambda_g) = \left(\mathbf{H}^H\mathbf{H} + \mathbf{\Lambda}\right)^{-1}\mathbf{H}^H\mathbf{r} \tag{3.12}$$

where $\mathbf{\Lambda}$ is a diagonal matrix and given by

$$\mathbf{\Lambda} = \text{diag}\{\underbrace{\lambda_1, \ldots, \lambda_1}_{s_1}, \ldots, \underbrace{\lambda_g, \ldots, \lambda_g}_{s_g}\}. \tag{3.13}$$

Note that (3.12) is a minimizer of (3.11) only when $\mathbf{H}^H\mathbf{H} + \mathbf{\Lambda}$ is semidefinite. When $g = 1$, there is only one λ_1, and Eq. (3.13) reduces to the CLS solution in [22].

[1]Note that the CML is not maximum likelihood, even in the case where (3.9) is solved exactly.

When $\lambda_1 = \ldots = \lambda_g = \sigma_n^2$, the CML detector reduces to the MMSE detector (3.5). Compared with the CLS detector [22], our new relaxation is tighter and continuous space is smaller.

In order to obtain the CML solution in (3.12), the optimal values for $\lambda_1, \ldots, \lambda_g$ have to be computed so that the unitary constraints are fulfilled. Substituting $\hat{\mathbf{x}}(\lambda_1, \ldots, \lambda_g)$ into (3.10), we need the zeros of the set of equations:

$$\begin{aligned} F_1(\lambda_1, \ldots, \lambda_g) &= \|\hat{\mathbf{x}}_1(\lambda_1, \ldots, \lambda_g)\|^2 - s_1 = 0 \\ &\vdots \\ F_g(\lambda_1, \ldots, \lambda_g) &= \|\hat{\mathbf{x}}_g(\lambda_1, \ldots, \lambda_g)\|^2 - s_g = 0. \end{aligned} \tag{3.14}$$

However, the solution of (3.14) does not necessarily guarantee that $\mathbf{H}^H\mathbf{H} + \mathbf{\Lambda}$ is semidefinite. Therefore, solving (3.14) does not guarantee the optimal solution of (3.10).

The multidimensional Newton-Raphson root finding method [56] can be used to solve (3.14). This method needs the partial derivative of F_i with respect to λ_j, $\partial F_i/\partial\lambda_j$, $1 \leq i, j \leq g$. For simplicity, only the differentiation of F_1 with respect to λ_1 and that of F_g with respect to λ_1 are shown. $\partial F_i/\partial\lambda_i$ can be obtained by permuting the columns of $\mathbf{H}$ such that $\mathbf{x}_i$ corresponds to the first s_i entries of $\mathbf{x}$. $\partial F_i/\partial\lambda_j$, $j \neq i$ can be obtained by permuting the columns of $\mathbf{H}$ such that $\mathbf{x}_i$ corresponds to the last s_i entries of $\mathbf{x}$ and $\mathbf{x}_j$ corresponds to the first s_j entries of $\mathbf{x}$. We can obtain $\partial F_1/\partial\lambda_1$

$$\begin{aligned} &\frac{\partial F_1(\lambda_1, \cdots, \lambda_g)}{\partial \lambda_1} \\ =&\mathbf{r}^H\mathbf{H} \begin{pmatrix} -2\mathbf{Q}^{-3} & \mathbf{Q}^{-2}\mathbf{B}\mathbf{C}^{-1}\mathbf{Q}^{-1} + \mathbf{Q}^{-1}\mathbf{B}\mathbf{C}^{-1}\mathbf{Q}^{-2} \\ \mathbf{Q}^{-2}\mathbf{C}^{-1}\mathbf{B}^H\mathbf{Q}^{-1} + \mathbf{Q}^{-1}\mathbf{C}^{-1}\mathbf{B}^H\mathbf{Q}^{-2} & -\mathbf{Q}^{-2}\mathbf{B}\mathbf{C}^{-2}\mathbf{B}^H\mathbf{Q}^{-1} - \mathbf{Q}^{-1}\mathbf{B}\mathbf{C}^{-2}\mathbf{B}^H\mathbf{Q}^{-2} \end{pmatrix} \mathbf{H}^H\mathbf{r}, \end{aligned} \tag{3.15}$$

where $\mathbf{A} = \mathbf{H}_1^H\mathbf{H}_1 + \lambda_1\mathbf{I}$, $\mathbf{B} = \mathbf{H}_1^H\mathbf{H}_2$, $\mathbf{C} = \mathbf{H}_2^H\mathbf{H}_2 + \Lambda_2$, $\Lambda_2 = \mathrm{diag}(\lambda_2, \ldots, \lambda_2, \ldots, \lambda_g, \ldots, \lambda_g)$, $\mathbf{Q} = \mathbf{A} - \mathbf{B}\mathbf{C}^{-1}\mathbf{B}^H$, $\mathbf{H}_1$ corresponds the first s_1 columns of $\mathbf{H}$, and $\mathbf{H}_2$ corresponds the last $n - s_1$ columns of $\mathbf{H}$. We also have

$$\frac{\partial F_g(\lambda_1, \cdots, \lambda_g)}{\partial \lambda_1} = \mathbf{r}^H\mathbf{H} \begin{pmatrix} \mathbf{\Phi} & \mathbf{\Psi} \\ \mathbf{\Omega} & \mathbf{\Xi} \end{pmatrix} \mathbf{H}^H\mathbf{r}, \tag{3.16}$$

where

$$\mathbf{\Phi} = -\mathbf{E}^H\mathbf{D} - \mathbf{D}^H\mathbf{E}, \tag{3.17}$$

$$\mathbf{\Psi} = -\mathbf{E}^H\mathbf{C}^{-1} - \mathbf{E}^H\mathbf{C}^{-1}\mathbf{B}^H\mathbf{D}^H - \mathbf{D}^H\mathbf{C}^{-1}\mathbf{B}^H\mathbf{E}^H, \tag{3.18}$$

$$\mathbf{\Omega} = -\mathbf{C}^{-1}\mathbf{E}^H - \mathbf{D}\mathbf{B}\mathbf{C}^{-1}\mathbf{E} - \mathbf{E}\mathbf{B}\mathbf{C}^{-1}\mathbf{D}, \tag{3.19}$$

$$\mathbf{\Xi} = -\mathbf{C}^{-2}\mathbf{B}^H\mathbf{E}^H - \mathbf{E}\mathbf{B}\mathbf{C}^{-2} - \mathbf{E}\mathbf{B}\mathbf{C}^{-2}\mathbf{B}^H\mathbf{D}^H - \mathbf{D}\mathbf{B}\mathbf{C}^{-2}\mathbf{B}^H\mathbf{E}^H, \tag{3.20}$$

$\mathbf{A} = \mathbf{H}_1^H\mathbf{H}_1 + \Lambda_1\mathbf{I}$, $\mathbf{B} = \mathbf{H}_1^H\mathbf{H}_2$, $\mathbf{C} = \mathbf{H}_2^H\mathbf{H}_2 + \lambda_g\mathbf{I}$, $\Lambda_1 = \mathrm{diag}(\lambda_1, \ldots, \lambda_1, \ldots, \lambda_{g-1}, \ldots, \lambda_{g-1})$, $\mathbf{Q} = \mathbf{A} - \mathbf{B}\mathbf{C}^{-1}\mathbf{B}^H$, $\mathbf{H}_1$ corresponds the first $n - s_g$ columns of $\mathbf{H}$, $\mathbf{H}_2$ corresponds the last s_g columns of $\mathbf{H}$, $\mathbf{\Delta} = \mathrm{diag}(\underbrace{1, \ldots, 1}_{s_1}, \ldots, 0, \ldots, 0)$, $\mathbf{E} = \mathbf{C}^{-1}\mathbf{B}^H\mathbf{Q}^{-1}\mathbf{\Delta}\mathbf{Q}^{-1}$, and $\mathbf{D} = \mathbf{C}^{-1}\mathbf{B}^H\mathbf{Q}^{-1}$.

There are several sets of roots for (3.14) and an initial estimate is needed to guarantee the convergence to the desired root. In the CLS case, where only λ_1 exists, from [57], it was shown that the global minimum is achieved by the maximal real root λ_1^*, which can be found using one-dimensional Newton method. But in the multidimensional case, no such theorem exists that specifies the root that minimizes (3.10). There are two possible initial estimates for λ_i. First, since the MMSE detector (3.5) provides a good solution, the initial values for λ_i are chosen as $\lambda_1 = \ldots = \lambda_g = \sigma_n^2$. Second, the CLS is solved first and the solution λ_1^* for $g = 1$ is used as the intimal estimate. If the Newton method does not converge after a specified number of iterations, we simply set $\lambda_1 = \ldots = \lambda_g = \sigma_n^2$ or $\lambda_1 = \ldots = \lambda_g = \lambda_1^*$, and the CML detector outputs the MMSE or CLS solution. Our simulation results show that the probability that the Newton method does not converge increases with the increase of g, which means that the probability that (3.14) does not have a solution increases. Since the Newton-Raphson root finding method returns the root close to the initial estimate, the global minimum of (3.10) may not be achieved by the root. Therefore, our approach is suboptimal for solving (3.10). However, based on our simulation results we find that if the CLS solution is used as the initial estimate, our detector always performs better than the original CLS detector.

For a non-unitary constellation such as QAM, we assume $\rho_{\max}$ and $\rho_{\min}$ as the

largest and smallest modulus of the constellation, respectively. As before, the vector $\mathbf{x}$ is partitioned into g groups and the constraint $\rho_{\max}$ is applied on each group. Thus each $\mathbf{x}_i$ is relaxed within a s_i-dimensional hypersphere $\mathbf{x}_i^H \mathbf{x}_i \leq \rho_{\max}^2 s_i$. The CML detector is modified as

$$\hat{\mathbf{x}}_{\mathrm{CML}} = D\left[\underset{\mathbf{x}_1^H\mathbf{x}_1 \leq \rho_{\max}^2 s_1, \ldots, \mathbf{x}_g^H \mathbf{x}_g \leq \rho_{\max}^2 s_g}{\arg\min} \|\mathbf{r} - \mathbf{H}\mathbf{x}\|^2\right]. \tag{3.21}$$

The Lagrangian function for the minimization problem in (3.21) can be expressed as

$$\mathcal{L}(\mathbf{x}, \lambda_1, \ldots, \lambda_g) = \|\mathbf{r} - \mathbf{H}\mathbf{x}\|^2 + \sum_{i=1}^{g} \lambda_i \left(\mathbf{x}_i^H \mathbf{x}_i - \rho_{\max}^2 s_i\right) \tag{3.22}$$

where λ_i is the Lagrangian multiplier associated with the ith inequality constraint, and $\lambda_i \geq 0$. The Lagrange dual function is the minimum value of the Lagrangian over (3.22) $\mathbf{x}$ and

$$g(\lambda_1, \ldots, \lambda_g) = \inf_{\mathbf{x} \in \mathbb{C}^n} \mathcal{L}(\mathbf{x}, \lambda_1, \ldots, \lambda_g) \tag{3.23}$$

Minimization of (3.22) for $\mathbf{x}$ has the same solution as (3.13). Substituting it back to (3.22), we obtain

$$g(\lambda_1, \ldots, \lambda_g) = -\mathbf{r}^H \mathbf{H} \left(\mathbf{H}^H \mathbf{H} + \mathbf{\Lambda}\right)^{-1} \mathbf{H}^H \mathbf{r} - \rho_{\max}^2 \sum_{i=1}^{g} \lambda_i s_i,\ \lambda_i \geq 0. \tag{3.24}$$

Both the objective function and the constraints are convex. There exists a strictly feasible point. Therefore, the constraints meet the Slater's condition and strong duality holds for (3.21) [58]. The maximum value of $g(\lambda_1, \ldots, \lambda_g)$ is equal to the minimum of (3.21). $\lambda_1, \ldots, \lambda_g$ is solved by maximizing (3.24) first, and substitute them back into (3.12) to obtain the solution to (3.21). In (3.24), the set $S = \{[\lambda_1, \ldots, \lambda_i] | \lambda_i \geq 0,\ i = 1, \ldots, g\}$ is convex. A g-dimensional subgradient algorithm [59] can thus be used to solve (3.24). For simplicity, we only show the differentiation of $g(\lambda_1, \ldots, \lambda_g)$ with respect to λ_1. $\partial g / \partial \lambda_i$, $i > 1$, can be obtained by permuting the columns of $\mathbf{H}$ such that $\mathbf{x}_i$ corresponds to the first s_i entries of $\mathbf{x}$. We can obtain

$$\frac{g(\partial\lambda_1, \ldots, \lambda_g)}{\partial \lambda_1} = \mathbf{r}^H \mathbf{H} \begin{pmatrix} \mathbf{Q}^{-2} & -\mathbf{Q}^{-2}\mathbf{B}\mathbf{C}^{-1} \\ -\mathbf{C}^{-1}\mathbf{B}^H\mathbf{Q}^{-2} & \mathbf{C}^{-1}\mathbf{B}^H\mathbf{Q}^{-2}\mathbf{B}\mathbf{C}^{-1} \end{pmatrix} \mathbf{H}^H \mathbf{r} - \rho_{\max}^2 s_1, \tag{3.25}$$

where $\mathbf{B}$, $\mathbf{C}$ and $\mathbf{Q}$ are defined in (3.15). The gradient descent algorithm starts at $\lambda_1 = \lambda_2 \ldots = \lambda_g = \sigma_n^2$. With dimenishing stepsize, the gradient descent algorithm converges to the optimal solution [59]. If $g = 1$, the CML detector (3.21) reduces to the GMMSE in [44]. Therefore, the CML detector is a generalization of the GMMSE.

For tighter constraints and better performance, $\rho_{\min}$ can also be considered by posing another g constraints $\rho_{\min}^2 s_i \leq \mathbf{x}_i^H \mathbf{x}_i$, for $i = 1, \ldots, g$ on (3.21). But the resulting optimization problem is non-convex, which is hard to solve in general.

Remarks:

- Eq. (3.12) reduces to the ZF detector if $\mathbf{\Lambda} = \mathbf{0}$.
- The constrained detectors that use constellation modulus information can be combined with the real constraint in 3.2.2. For real constellations, the CML detectors (3.9) and (3.21) can be directly applied to the equivalent system (3.6) by taking into account both the real and modulus constraints. The combined receiver is denoted as R-CML.
- The proposed approach can also be extended to MMSE equalizers. Let the prefilter matrix in MMSE be $\mathbf{G}$ and the prefilter output be $\hat{\mathbf{x}} = \mathbf{G}\mathbf{r}$. Denote $\mathcal{P}$ as the average constellation power. The constrained MMSE equalizer can be obtained by solving

$$\min_{\mathbf{G}} E\{\|\mathbf{x} - \hat{\mathbf{x}}\|^2\}, \text{ s.t. } E\{\hat{\mathbf{x}}_1^H \hat{\mathbf{x}}_1\} = s_1 \mathcal{P}, \ldots, E\{\hat{\mathbf{x}}_g^H \hat{\mathbf{x}}_g\} = s_g \mathcal{P}. \tag{3.26}$$

  The details of solving (3.26) is omitted here.

3.2.4 Coordinate Ascent Improvement

Although the proposed detectors perform inferior to the MLD, in high SNR they usually have only one or two symbol errors (i.e., $\tilde{x}_k = x_k$ for most k and for unreliable decisions $\tilde{x}_k \neq x_k$). We thus propose using an iterative detector to improve the performance of our constrained detectors by correcting some unreliable decisions,

which is a block version of a coordinate ascent algorithm [56]. As before with the CML detectors, $\mathbf{x}$ is partitioned into g groups each with s_i symbols. In each iteration, for $i = 1, \ldots, g$, we minimize one group by fixing the other $g-1$ groups. The algorithm can be summarized in the following two steps:

- Initialization: Set iteration number $k = 0$ and obtain the initial data detection using a suboptimal detector. This initial solution is denoted as $\hat{\mathbf{x}}^{(0)}$.

- Iteration: $k = k + 1$ and set iteration number $i = 1$.

  for $i = 1 : g$, compute

  $$\mathbf{r}^{(i)} = \mathbf{r} - \mathbf{H}_{\bar{i}}\hat{\mathbf{x}}^{(k-1)} \tag{3.27}$$

  where $\mathbf{H}_{\bar{i}}$ is formed by zeroing the columns from $f_i = \sum_{j=1}^{i-1} s_j + 1$ to $e_i = \sum_{j=1}^{i} s_j$. The data vector $\mathbf{x}_i = [x_{f_i}, \ldots, x_{e_i}]^T$ is detected using

  $$\hat{\mathbf{x}}_i = \arg\min_{\mathbf{x}_i \in \mathcal{Q}^{s_i}} \left\| \mathbf{r}^{(i)} - \mathbf{H}_i \mathbf{x}_i \right\|^2 \tag{3.28}$$

  where $\mathbf{H}_i$ is formed by the columns from f_i to e_i.

  $\hat{\mathbf{x}}^{(k)} = [\hat{\mathbf{x}}_1, \ldots, \hat{\mathbf{x}}_g]^T$ and the iteration continues until $\hat{\mathbf{x}}^{(k)} == \hat{\mathbf{x}}^{(k-1)}$.

Remarks:

- When the number of groups g varies from 1 to n, different performance levels ensue. In particular, if $g = 1$, (3.28) reduces to the maximum likelihood detection problem (3.2). When $g = n$, the iterative improvement algorithm is similar to the parallel interference cancellation (PIC) detector in CDMA systems. However, the iterative algorithm for MIMO with $g = n$ performs worse than PIC in CDMA due to the following reason. In the CDMA case, the non-diagonal terms in $\mathbf{H}$ due to the non-orthogonality of the spreading codes are typically small, which does not hold for the MIMO channel $\mathbf{H}$. Our new iterative improvement, however, generalizes the PIC detector.

- When s_i is small, exhaustive search can solve (3.28), or it may be solved by the SD with reduced complexity. In any case, the worst-case complexity of our new iterative algorithm is $O(K\sum_{i=1}^{g}|Q|^{s_i})$, where K is the total number of iterations. The complexity is also between those of the SD and PIC. How to choose g and s_i depends on many factors. For example, it depends on the suboptimal detector or equalizer used, and the desired BER and complexity. Note that for practical system design, g and s_i can be chosen empirically to achieve a good performance-complexity tradeoff at a given SNR.

- For soft decoding of linear block codes, Chase has proposed a class of suboptimal decoders [60]. Different versions of the Chase detector have also been developed for MIMO detection [61, 62].

- From [45, 63], the diversity order of the first few detected symbols is less than that of the later detected symbols, and the overall performance is limited by the first few symbols. Therefore, $s_1, \ldots, s_g$ should be in decreasing order to correct the errors in early stages.

3.3 Constrained Decision Feedback Detectors

3.3.1 V-BLAST Detection

The V-BLAST detection algorithm [13] relies on nulling and interference cancellation. Nulling is performed by linearly weighting the received symbols to satisfy the ZF or MMSE criterion. For interference cancellation, the effect of previously-detected symbols can be subtracted from the samples for the symbols yet to be detected. This improves the overall performance when the order of detection is chosen carefully. The detection process consists of n iterations. In the k-th iteration, the signal with maximum post-detection SNR among the remaining $n-k+1$ symbols is detected, which is known to be the optimal detection order. The whole algorithm is described as follows:

- Initialization:

$$\begin{aligned} \mathbf{r}_1 &= \mathbf{r} && (3.29a)\\ \mathbf{G}_1 &= \mathbf{H}^\dagger && (3.29b)\\ k_1 &= \arg\min_j \|(\mathbf{G}_1)_j\|^2 && (3.29c) \end{aligned}$$

- Recursion: for $i = 1$ to n

$$\begin{aligned} \mathbf{w}_{k_i} &= (\mathbf{G}_i)_{k_i} && (3.29d)\\ \hat{x}_{k_i} &= \arg\min_{x\in\mathcal{Q}} \left|x - \mathbf{w}_{k_i}^H \mathbf{r}_i\right|^2 && (3.29e)\\ \mathbf{r}_{i+1} &= \mathbf{r}_i - \hat{x}_{k_i}(\mathbf{H})_{k_i} && (3.29f)\\ \mathbf{G}_{i+1} &= \mathbf{H}_{\bar{k_i}}^\dagger && (3.29g)\\ k_{i+1} &= \arg\min_{j\notin\{k_1,\ldots,k_i\}} \|(\mathbf{G}_{i+1})_j\|^2 && (3.29h) \end{aligned}$$

where $(\mathbf{A})_i$ is the i-th column of matrix $\mathbf{A}$ and $\mathbf{H}_{\bar{k_i}}$ is obtained by zeroing the $k_1, \ldots, k_i$-th columns of $\mathbf{H}$.

As suggested in [46], given an optimum order $k_1, \ldots, k_n$, V-BLAST detection is equivalent to the ZF-DFD. Assuming $\mathbf{\Pi}$ is the column permutation matrix obtained from the optimum order, we apply $\mathbf{\Pi}$ to $\mathbf{H}$[2]. Let the QR factorization of $\tilde{\mathbf{H}} = \mathbf{H}\mathbf{\Pi}$ be $\mathbf{QR}$, where $\mathbf{Q}$ is a unitary matrix and $\mathbf{R}$ is an upper-triangular one. Eq. (3.1) is equivalent to

$$\mathbf{y} = \mathbf{R}\mathbf{x} + \mathbf{v} \tag{3.30}$$

where $\mathbf{y} = \mathbf{Q}^H\mathbf{r}$ and $\mathbf{v} = \mathbf{Q}^H\mathbf{n}$ is also an i.i.d. complex Gaussian vector with mean zero and variance σ_n^2. The second description of V-BLAST algorithm is given by

- for $i = n$ to 1

$$\begin{aligned} \hat{x}_i &= \arg\min_{x\in\mathcal{Q}} |y_i - R_{i,i}x|^2 && (3.31a)\\ \mathbf{y} &= \mathbf{y} - (\mathbf{R})_i\hat{x}_i && (3.31b) \end{aligned}$$

[2]As in [46], the filtering matrices in constrained detectors and the corresponding constrained ordering can be applied similarly.

end

where $R_{i,i}$ is the (i,i)-th entry of $\mathbf{R}$, and $(\mathbf{R})_i$ is the i-th column of $\mathbf{R}$.

3.3.2 Real Decision Feedback Detectors

For real valued constellations, the V-BLAST algorithm (3.29a)-(3.29h) is performed on the real system (3.6), which automatically takes the real constraint into account. V-BLAST for (3.6) is denoted as R-V-BLAST. Using the same arguments in 3.2.2, R-V-BLAST performs better than the original V-BLAST by suppressing the imaginary interference. More precisely, if $n = m$ and no permutations are used, the squared-norm of the entries of $\mathbf{R}$ are known to be χ^2 distributed [64], specifically, $|R_{i,i}|^2 \sim \chi^2(2i)$, for $i = 1, \ldots, n$ and $|R_{i,j}|^2 \sim \chi^2(2)$, for $j > i$, where $\chi^2(k)$ denotes the chi-squared distribution with k degrees of freedom. Since the performance of V-BLAST is limited by the first detected symbol [45], the diversity order of V-BLAST detection is only one [65,66]. However, if QR decomposition is performed on the $2n \times n$ real matrix $\tilde{\mathbf{H}}$ in (3.6), we first construct a $2n \times 2n$ real matrix $\mathbf{H}_1$ with each entry zero mean and variance 1 and the first n columns are equal to $\tilde{\mathbf{H}}$. Let the QR decomposition $\tilde{\mathbf{H}}$ and $\mathbf{H}_1$ be $\tilde{\mathbf{H}} = \tilde{\mathbf{Q}}\tilde{\mathbf{R}}$ and $\mathbf{H}_1 = \mathbf{Q}_1\mathbf{R}_1$, and $|R_{i,i}|^2 \sim \chi^2(i)$, for $i = 1, \ldots, 2n$ and $|R_{i,j}|^2 \sim \chi^2(1)$, for $j > i$. We have $\mathbf{R}_2 = \tilde{\mathbf{H}}\mathbf{Q}_1^H$, which consists of the first n columns of $\mathbf{R}_1$. Therefore the squared-norm of the entries of $\tilde{\mathbf{R}}$ are also χ^2 distributed but $|\tilde{R}_{i,i}|^2 \sim \chi^2(i+n)$, for $i = 1, \ldots, n$ and $|\tilde{R}_{i,j}|^2 \sim \chi^2(1)$, for $j > i$. Therefore, using the analysis approach in [45, 63], it can be readily verified that the diversity order of R-V-BLAST increases to $(n+1)/2$. For real constellations, by using the decoupled system with real constraint (3.6), the diversity order increases from 1 to $(n+1)/2$, which has significant performance gain over the original V-BLAST. This also shows a diversity rate trade-off.

For decoupleable complex constellations i.e., QAM, (3.1) can be rewritten as

$$\begin{bmatrix} \mathrm{Re}\{\mathbf{r}\} \\ \mathrm{Im}\{\mathbf{r}\} \end{bmatrix} = \begin{bmatrix} \mathrm{Re}\{\mathbf{H}\} & -\mathrm{Im}\{\mathbf{H}\} \\ \mathrm{Im}\{\mathbf{H}\} & \mathrm{Re}\{\mathbf{H}\} \end{bmatrix} \begin{bmatrix} \mathrm{Re}\{\mathbf{x}\} \\ \mathrm{Im}\{\mathbf{x}\} \end{bmatrix} + \begin{bmatrix} \mathrm{Re}\{\mathbf{n}\} \\ \mathrm{Im}\{\mathbf{n}\} \end{bmatrix} \tag{3.32}$$

or

$$\tilde{\mathbf{r}} = \tilde{\mathbf{H}}\tilde{\mathbf{x}} + \tilde{\mathbf{n}}. \tag{3.33}$$

In [67], it has been shown that applying V-BLAST to the equivalent real system (3.32) yields an additional performance gain. However, diversity order is not increased. These suggest that it is always beneficial to perform V-BLAST algorithm on the equivalent real system if the constellation is decoupleable or real.

3.3.3 Constrained Ordering Decision Feedback Detectors

The ZF nulling vector $\mathbf{w}_{k_i}$ (3.29d) in V-BLAST completely removes the interferences from the other antennas but also amplifies the additive noise. Instead of using $\mathbf{w}_i$ in (3.29d) to remove completely the interference, we use a non complete nulling vector for a better tradeoff between noise enhancement and interference suppression. We propose using the filtering matrix in our proposed constrained detectors in 3.2 as nulling vector instead of the ZF nulling vector in V-BLAST. We replace (3.29b) and (3.29g) with

$$\mathbf{G}_1 = \left(\mathbf{H}^H\mathbf{H} + \mathbf{\Lambda}\right)^{-1}\mathbf{H}^H \tag{3.34}$$

and

$$\mathbf{G}_{i+1} = \left(\mathbf{H}_{\bar{k}_i}^H\mathbf{H}_{\bar{k}_i} + \mathbf{\Lambda}_i\right)^{-1}\mathbf{H}_{\bar{k}_i}^H \tag{3.35}$$

where $\mathbf{\Lambda}$ and $\mathbf{\Lambda}_i$ can be calculated using (3.14) and (3.24) for constant unitary and non-unitary constellations, respectively.

Since interference cannot be removed completely when nulling is performed using CML, we propose to determine the detection order at each iteration by maximizing the SINR defined as

$$\mathrm{SINR}_j = \frac{|(\mathbf{G}_{i+1}\mathbf{H}_{\bar{k}_i})_{j,j}|^2 E\{|x_j|^2\}}{\sum_{k=1,k\neq j}^{n}|(\mathbf{G}_{i+1}\mathbf{H}_{\bar{k}_i})_{j,k}|^2 E\{|x_k|^2\} + \sigma_n^2\|(\mathbf{G}_{i+1})_j\|^2} \tag{3.36}$$

where $(\mathbf{A})_{i,j}$ is the (i,j)-th entry of matrix $\mathbf{A}$ and $(\mathbf{G}_{i+1})_j$ denotes the j-th row of matrix $\mathbf{G}_{i+1}$. In the V-BLAST detection algorithm, (3.29h) is replaced by

$$k_{i+1} = \underset{j\notin\{k_1,\ldots,k_i\}}{\arg\max}\ \mathrm{SINR}_j. \tag{3.37}$$

This modified V-BLAST detection is denoted as constrained ordering DFD (CODFD).

Note that if $\mathbf{\Lambda} = \sigma_n^2 \mathbf{I}_n$, CODFD reduces to MMSE-DFD in [47]. If $\mathbf{\Lambda} = \mathbf{0}$, our CODFD becomes the original V-BLAST. Different ordering schemes with CML detectors and MMSE detectors can be combined to form hybrid ordering schemes. From [45, 63], the diversity order of the first few detected symbols is less than that of the later detected symbols. Since the CML detector with $g = n$ performs better than the other CML detectors and MMSE detector but with higher complexity, ordering can be performed with this detector in the first k symbols for a better tradeoff between noise enhancement and interference suppression. In the last $n - k$ stages, the original V-BLAST or MMSE-DFD ordering with low complexity can be applied since the diversity order in these stages is high. This hybrid ordering scheme gives a tradeoff between complexity and performance.

3.3.4 Combined Constrained and Decision Feedback Detectors

The performance of ZF-DFD, or equivalent V-BLAST, is limited by the error propagation of decision feedback. Even with the V-BLAST optimal ordering, the diversity order of V-BLAST detection is just one [65, 66]. This is because V-BLAST is a greedy algorithm. That is, a hard decision is made based only on the "local" metric (3.31a) without taking the subsequent symbol decisions into account. We thus combine the constrained detectors in 3.2 and the ZF-DFD in order to make hard decisions less greedily. At each iteration, a "global" metric is used to make decision on each symbol, which is obtained by the constrained detectors.

In the i-th iteration, define $\mathbf{R}_i = \mathbf{R}(1 : i-1, 1 : i-1)$, $\mathbf{r}_i = \mathbf{R}(1 : i-1, i)$ and $\mathbf{y}_i = \mathbf{y}(1 : i-1)$. For each $x \in \mathcal{Q}$, after cancelling x from $\mathbf{y}$, the soft decisions for the remaining $n - i$ symbols can be obtained using the constrained detectors as

$$\hat{\mathbf{x}}_i = \left(\mathbf{R}_i^H \mathbf{R}_i + \mathbf{\Lambda}_i\right)^{-1} \mathbf{R}_i^H (\mathbf{y}_i - \mathbf{r}_i x) \tag{3.38}$$

where $\mathbf{x}_i = [x_1, \ldots, x_{i-1}]^T$ and $\mathbf{\Lambda}_i$ is defined in (3.12). Since the solution to (3.10)

or (3.21) gives a low bound on $\|\mathbf{r}-\mathbf{H}\mathbf{x}\|^2$, the effect of x on the decision metric for the remaining $n-i$ symbols can be measured using $\|\mathbf{y}_i-\mathbf{r}_i x-\mathbf{R}_i\hat{\mathbf{x}}_i\|^2$. The global metric for x is defined as

$$\begin{aligned} M_i(x) =&\|\mathbf{y}_i-\mathbf{r}_i x-\mathbf{R}_i\hat{\mathbf{x}}_i\|^2+|y_i-R_{i,i}x|^2 \\ =&\left\|(\mathbf{I}_{n-i}-\mathbf{R}_i(\mathbf{R}_i^H\mathbf{R}_i+\mathbf{\Lambda}_i)^{-1}\mathbf{R}_i^H)(\mathbf{y}_i-\mathbf{r}_i x)\right\|^2+|y_i-R_{i,i}x|^2 \\ =&|a_i-b_i x|^2 \end{aligned} \quad , \tag{3.39}$$

where

$$\begin{aligned} a_i =&\sqrt{\|(\mathbf{I}_{n-i}-\mathbf{R}_i(\mathbf{R}_i^H\mathbf{R}_i+\mathbf{\Lambda}_i)^{-1}\mathbf{R}_i^H)\mathbf{r}_i\|^2+|R_{i,i}|^2} \\ b_i =&\left(\mathbf{y}_i^H(\mathbf{I}_{n-i}-\mathbf{R}_i(\mathbf{R}_i^H\mathbf{R}_i+\mathbf{\Lambda}_i)^{-1}\mathbf{R}_i^H)^2\mathbf{r}_i+y_i^*R_{i,i}\right)/a_i. \end{aligned} \tag{3.40}$$

In the ZF-DFD, (3.31a) is simply replaced by

$$\hat{x}_i = D\left[\arg\min_{x\in\mathcal{Q}} M_i(x)\right]. \tag{3.41}$$

The resulting detector is denoted by CML-DFD. With pre-computed a_i and b_i, the total complexity of CML-DFD is still $O(n^3)$.

Remarks:

- If the CML detector is used, from the duality theory [58], $\|\mathbf{y}_i-\mathbf{r}_i x-\mathbf{R}_i\hat{\mathbf{x}}_i\|^2$ gives a lower bound and it measures the effect of x on the remaining symbols.

- If $\mathbf{\Lambda}_i=\sigma_n^2\mathbf{I}_{n-i}$, (3.38) reduces to MMSE. Though it does not give a lower bound on $\|\mathbf{y}_i-\mathbf{r}_i x-\mathbf{R}_i\hat{\mathbf{x}}_i\|^2$, the metric (3.39) also measures the effect of x on the overall metric. Therefore, the combined MMSE and DFD (CMMSE-DFD) enhances the performance.

- The terms $\|\mathbf{y}_i-\mathbf{r}_i x-\mathbf{R}_i\hat{\mathbf{x}}_i\|^2$ and $|y_i-R_{i,i}x|^2$ are equally weighted in (3.39). However, the two terms may be weighed differently, and (3.39) can then be written as

$$M_i(x) = w_i\|\mathbf{y}_i-\mathbf{r}_i x-\mathbf{R}_i\hat{\mathbf{x}}_i\|^2+(1-w_i)\,|y_i-R_{i,i}x|^2\,, \tag{3.42}$$

where $0 \leq w_i \leq 1$ is the weight coefficient. If $w_i = 0.5$, (3.42) is equivalent to (3.39). If $w_i = 0$, (3.42) reduces to (3.31b), and the CML-DFD becomes ZF-DFD. The coefficient w_i can be optimized by minimizing the MSE for x_i. In practice, w_i may be found by simulation.

- When the channel varies rapidly, the coefficients a_i and b_i must be updated frequently, thereby increasing the average complexity of the detector. To alleviate this computation burden, the global metric (3.39) is used to detect the first k symbols and the original V-BLAST local metric (3.31b) for the remaining $n-k$ symbols. The parameter k offers a complexity-performance tradeoff.

3.4 Simulation results

Our proposed constrained detectors are tested for a MIMO system with 8 transmit and 8 receive antennas over a flat Rayleigh fading channel. The receiver has perfect channel state information (CSI) and noise variance. The notation CAI-X denotes the combination of the detector X and coordinate ascent iterative correction in 3.2.4. The system is simulated using MATLAB V7.0.4 on a workstation with an Intel Xeon processor at 3.2GHz. The average CPU computation time is used as the measure of complexity. The signal-to-noise ratio per bit is defined as

$$\frac{E_b}{N_0} = \frac{E\{\|\mathbf{Hx}\|^2\}}{m \log_2 |\mathcal{Q}| N_0}, \tag{3.43}$$

where N_0 is the spectral noise density. The SD is implemented using the algorithm in [48].

Fig. 3.1 shows the BER performance of different constrained detectors in a BPSK modulated system. Our detectors are compared with the MLD and the CLS detector [22]. When all the detectors are applied to the complex system (3.1), the CLS and CML perform close to MMSE. In high SNR, the CML with $g = 8$ performs better than MMSE. But all these detectors perform worse than the SD, which is optimal. When they are applied to the real system (3.6), all the detectors perform better. At

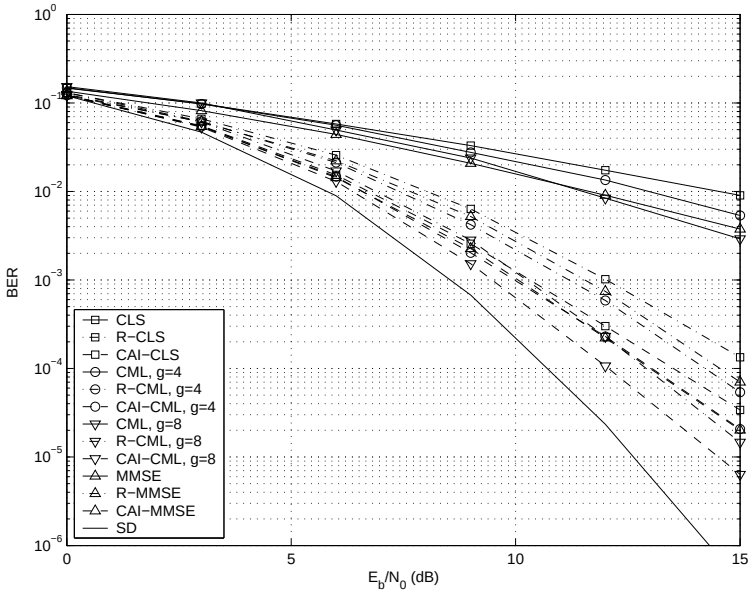

Fig. 3.1. Performance comparison of constrained detectors in an 8×8 MIMO system with BPSK.

a BER of 10^{-3}, R-MMSE has a 0.5 dB gain over R-CLS. Both R-CML with $g = 4$ and $g = 8$ perform better than R-MMSE. They have 0.3 dB and 2 dB gain over R-MMSE, respectively. After employing the iterative improvement to all the detectors, R-MMSE, R-CLS and R-CML with $g = 4$ have 2 dB, 1.8 dB and 1.5 dB gains at a BER of 10^{-3}. The detector R-CML with $g = 8$ improves by 1 dB at a BER of 10^{-4}.

The BER of GMMSE [44] and different constrained detectors for 16QAM is shown in Fig. 3.2. The GMMSE performs worst among all the detectors. CML with $g = 4$ has a 0.8 dB loss over MMSE at a BER of 10^{-3}. In low SNR, CML with $g = 8$ performs better than MMSE, but they perform identically in high SNR. With the Chase iterative improvement, R-MMSE, R-CLS, R-CML with $g = 4$ and R-CML with $g = 8$ have 2 dB, 1.8 dB, 1 dB and 1.2 dB gains at a BER of 10^{-2}, respectively. Since the group-wise hypersphere constraint (3.21) is loose, the resulting performance improvement is marginal. Tighter constraints are needed for high order QAM constellations.

Fig. 3.3 compares the BER of DFD and real DFD with different constrained ordering schemes. BPSK modulation is used. The performance of V-BLAST and the

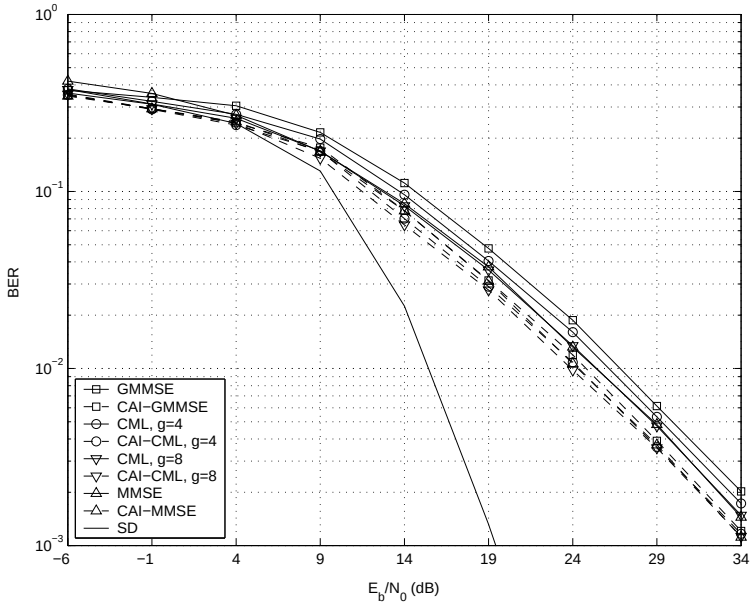

Fig. 3.2. Performance comparison of constrained detectors in an 8×8 MIMO system with 16QAM.

SD is also shown in Fig. 3.3. A dramatic performance improvement is observed even for the constrained DFDs on the complex model. At a BER of 10^{-2}, the CODFDs and MMSE-DFD have more than 3 dB gain over V-BLAST. Therefore, the CODFD and the MMSE-DFD have a smaller noise enhancement compared to the ZF-DFD. When the real constraint is imposed, R-V-BLAST and R-MMSE-DFD perform close to the SD at high SNR. They both perform only about 0.2 dB worse than the SD at a BER of 10^{-4}. The gap between R-CODFD with $g = 8$ and R-V-BLAST is 0.7 dB at a BER of 10^{-4}. Since the diversity order of R-V-BLAST is $(n + 1)/2$, it performs well and the performance improvement by using R-MMSE-DFD is small.

Fig. 3.4 shows the BER of DFD with different constrained ordering schemes for 16QAM. V-BLAST and the SD are used as benchmarks. The performance of R-V-BLAST using (3.33) is also presented. CODFD with $g = 1$ has only a 0.7 dB gain over V-BLAST at a BER of 10^{-3}, but it has a 0.8 dB loss over R-V-BLAST, which may be due to the loose hypercube relaxation (3.21). When $g = 8$, CODFD has a 2.7 dB loss over the SD at a BER of 10^{-3}. MMSE-DFD performs better than CODFD. At

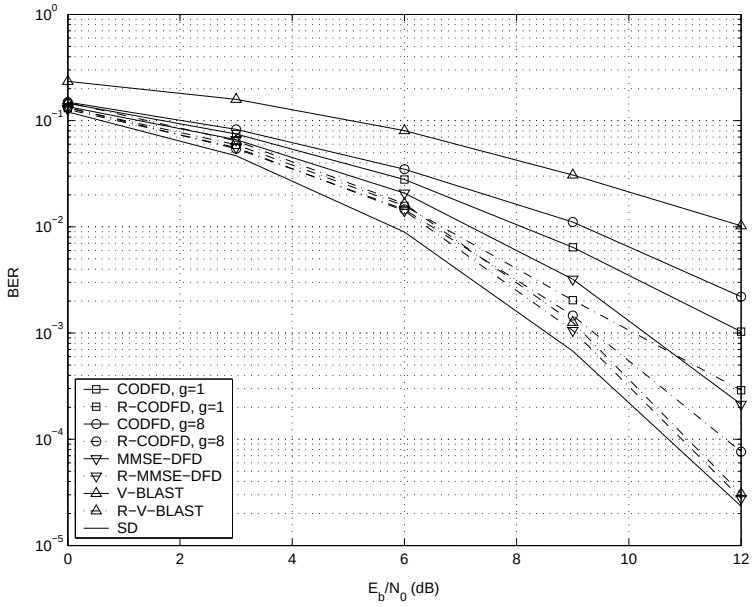

Fig. 3.3. Performance comparison of constrained ordering decision feedback detectors in an 8×8 MIMO system with BPSK.

a BER of 10^{-3}, MMSE-DFD only has a 1.5 dB loss over the SD. The gap reduces to 0.5 dB when R-MMSE-DFD is used. Therefore, R-MMSE-DFD is a preferable ordering scheme. However, all the order schemes only achieve a diversity order one, which may be caused by the greedy nature of the DFD.

The BERs of the combined constrained and decision feedback detectors for a BPSK system for different k are shown in Fig. 3.5, where k is the number of symbols detected using the global metric (3.39) and the remaining symbols are detected using the original V-BLAST local metric (3.31b). Our proposed CML-DFDs significantly improve the performance, indicating their ability to mitigate error propagation. The performance of all the combined detectors improves with k. At a BER of 10^{-2}, the CML-DFD with $g = 1$ and $k = 8$ has a 4 dB gain over V-BLAST. The CML-DFD performs better than the CMMSE-DFD with the same k. At a BER of 10^{-4}, the CML-DFD with $g = 8$ performs 0.5 dB better than the CMMSE-DFD when $k = 8$. The performance gain by increasing k diminishes with the increase of k. For CMMSE-DFD, 1.2 dB gain is achieved by increasing k from two to four at a BER of

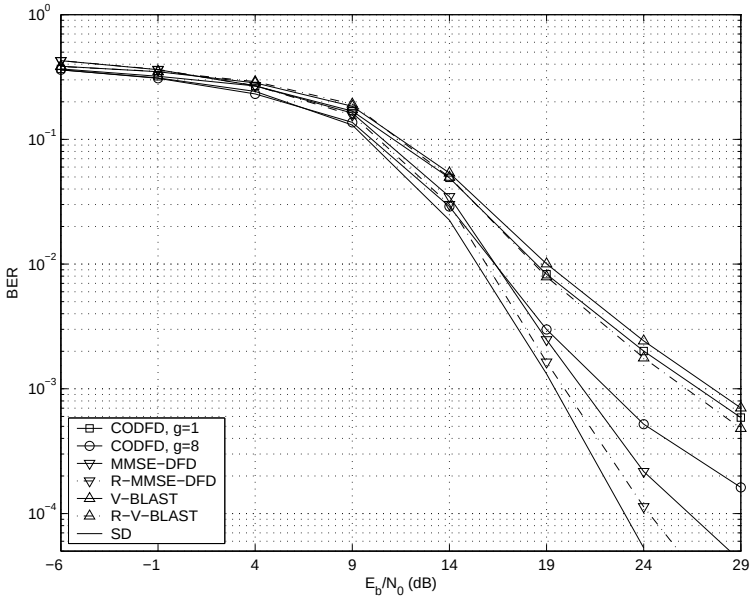

Fig. 3.4. Performance comparison of constrained ordering decision feedback detectors in an 8×8 MIMO system with 16QAM.

10^{-3}. However, the performance gain reduces to 0.2 dB when k increases from four to eight. The CML-DFD with $g = 8$ and $k = 8$ has the best performance among all the combined detectors and it performs only 2.2 dB worse than the SD at a BER of 10^{-3}.

Fig. 3.6 shows the average computational time of the SD and CMMSE-DFD for different k. The computational time of the SD is without counting the preprocessing. For CMMSE-DFD, the coefficients a_i and b_i are computed in each block, which is included in the computational time. The CMMSE-DFD has a constant complexity with the same k over all the SNRs, and its complexity increases with k. The CMMSE-DFD is faster than the SD in the observed SNR region. At SNR= 0 dB, CMMSE-DFD with $k = 2$ is 13 times faster than the SD. In practice, the choice $k = n/2$ achieves a good performance-complexity tradeoff.

Fig. 3.7 shows the performance of combined detectors for a BPSK system when the real constraint is applied. All the detectors perform close to the SD. R-CMMSE-DFD with $k = 1$ has only a 0.6 dB loss over the SD at a BER of 10^{-4}. R-CML-DFD

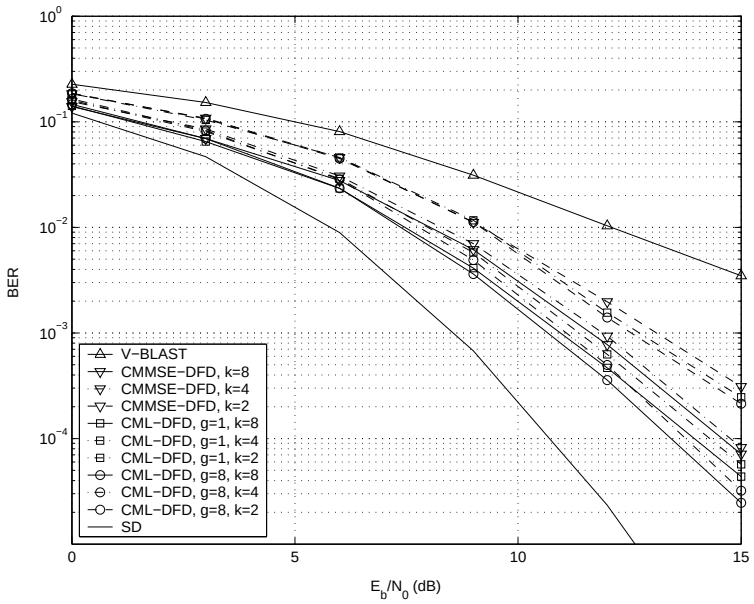

Fig. 3.5. Performance comparison of combined constrained and decision feedback detectors in an 8×8 BPSK MIMO system.

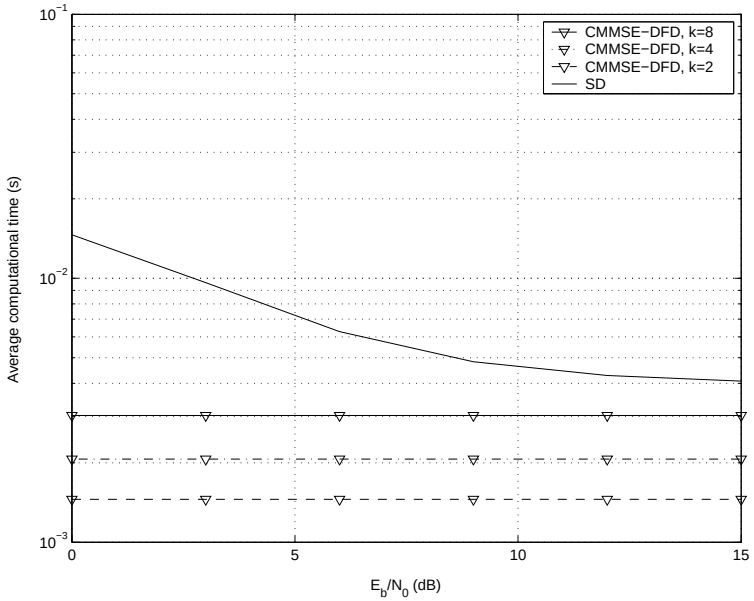

Fig. 3.6. Average computational time of combined constrained and decision feedback detectors in an 8×8 BPSK MIMO system.

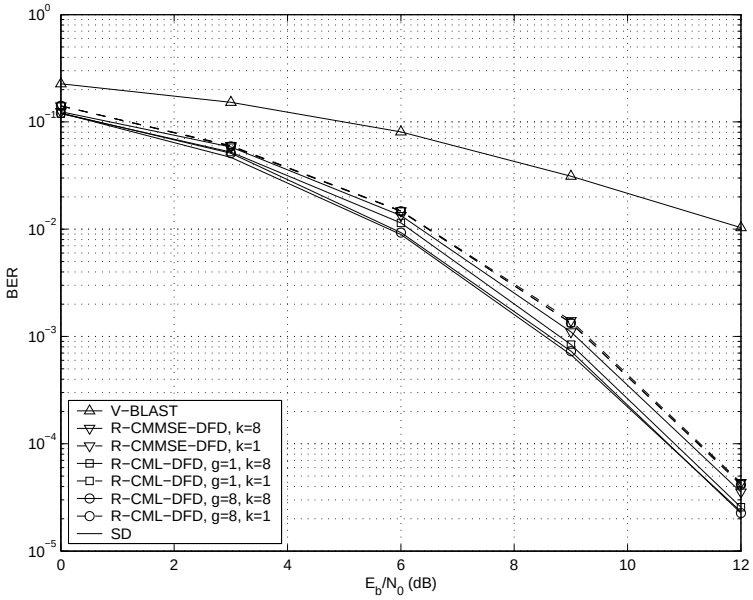

Fig. 3.7. Performance comparison of combined constrained and decision feedback detectors in an 8×8 BPSK MIMO system using real constraints.

with $g = 8$ and $k = 8$ almost achieves the maximum likelihood performance. However, the performance gain by increasing k decreases compared to the complex case in Fig. 3.7. Our combined detectors perform better than the V-BLAST detector.

Fig. 3.8 shows the average computational time of the SD and R-CMMSE-DFD. R-CMMSE-DFD is less complex than the SD for different SNR. Since only real operations are performed when solving the real system (3.32), R-CMMSE-DFD is less complex than the corresponding CMMSE-DFD, while the former performs better for the same k. R-CMMSE-DFD with $k = 1$ has a 16 times complexity saving over the SD at SNR$= 0\,$dB. When real constellations are used in practice, R-CMMSE-DFD with $k = 1$ is enough to achieve good performance with low complexity.

Fig. 3.9 compares the combined constrained and decision feedback detectors for a 16QAM system for different values of k. While the performance of all the combined detectors improves by increasing k, the improvement is not as significant as that for a BPSK system. At a BER of 3×10^{-3}, CMMSE-DFD with $k = 8$ has about $4\,$dB gain over V-BLAST. CML-DFD with $g = 1$ performs worse than CMMSE-DFD, and

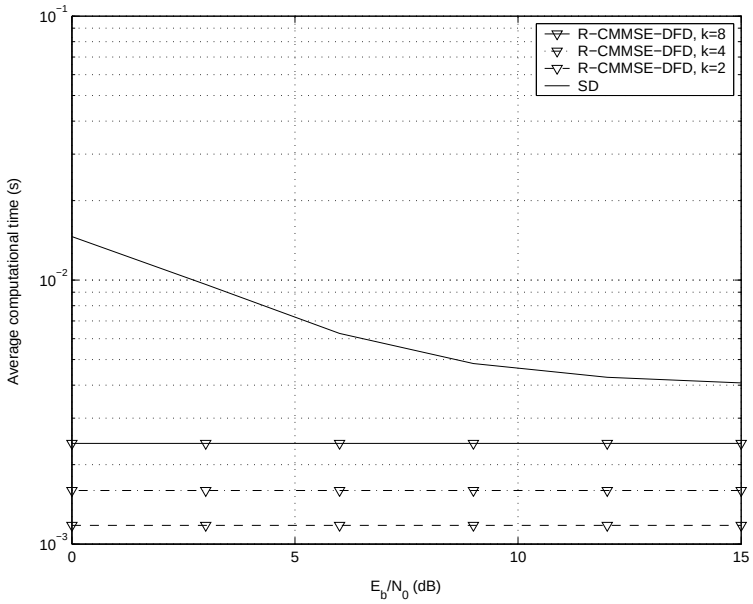

Fig. 3.8. Average computational time of combined constrained and decision feedback detectors in an 8×8 BPSK MIMO system using real constraints.

it has a 1 dB loss over CMMSE-DFD at a BER of 10^{-3}. CML-DFD with $g = 8$ and $k = 8$ achieves the best performance, and it almost reaches the benchmark by the SD. Therefore, the global metric given by CML-DFD with $g = 1$ is loose compared to the other two detectors.

Fig. 3.10 shows the average computational time of the SD and CMMSE-DFD for different k. The computational time of the SD is without counting the preprocessing. For CMMSE-DFD, the coefficients a_i and b_i are computed in each block, which is included in the computational time. Similarly, the CMMSE-DFD has a constant complexity for the same k over all the SNRs, and its complexity increases with k. In low SNR, CMMSE-DFD is less complex than the SD for all values of K. The SD has less complexity than CMMSE-DFD with $k = 8$ in high SNR (SNR$>$ 23 dB). In low SNR (SNR$<$ 15 dB), which is usually the case in practice, our CMMSE-DFD has $2-3$ orders of magnitude of complexity reduction over SD. For example, at SNR$=$ 5 dB, our CMMSE-DFD is 538 times faster than the SD. When the channel is static over several blocks and a_i, b_i can be precomputed, the resulting computational saving is

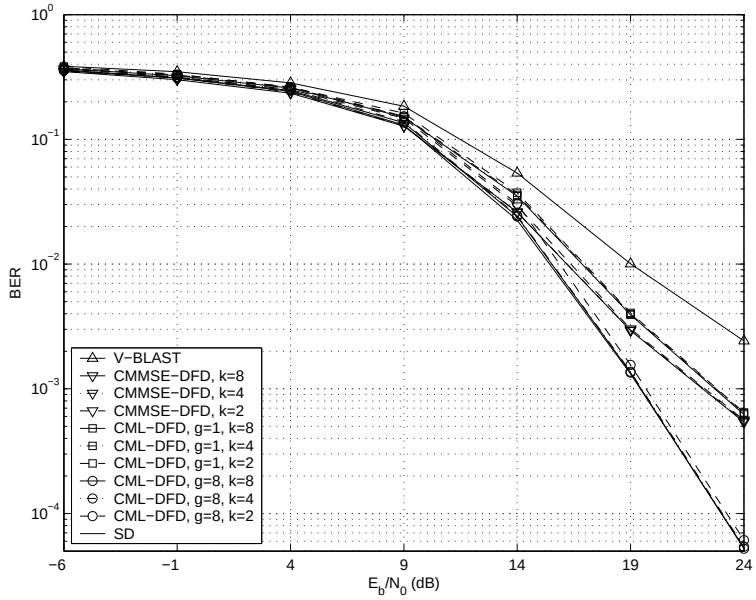

Fig. 3.9. Performance comparison of combined constrained and decision feedback detectors in an 8×8 16QAM MIMO system.

even more significant.

3.5 Summary

In this chapter, several constrained detectors and constrained decision feedback detectors have been proposed. Real constrained detectors are proposed to exploit the real-valued property of the real constellations such as BPSK. This is found to increase the diversity order to $(n+1)/2$. The previous CLS detector for OFDM/SDMA and GMMSE detector for CDMA were generalized as MIMO detectors for both unitary and non-unitary constellations. A coordinate ascent iterative technique has also been proposed to improve the performance of the proposed detectors. A constrained ordering scheme for DFDs has been derived to alleviate noise enhancement and to improve interference suppression. We also proposed combined constrained and decision feedback detectors, where a global metric is defined to mitigate the error propagation. The complexity of these combined detectors is reasonably low.

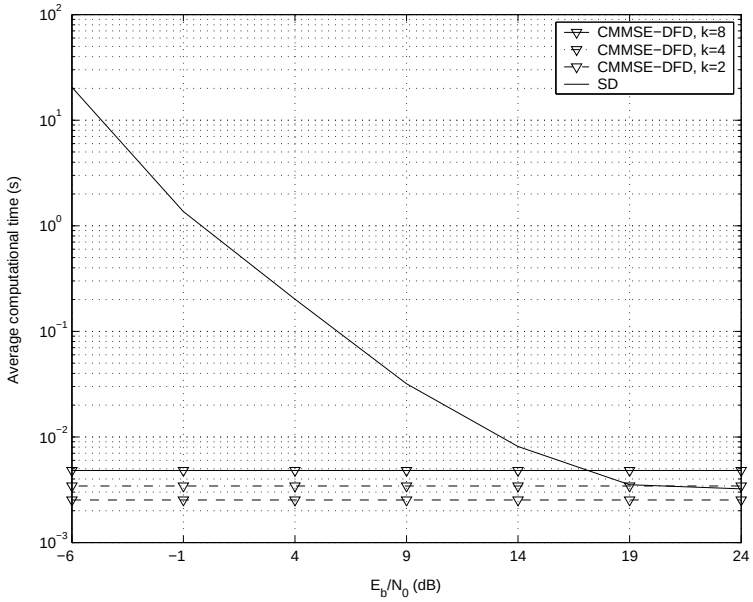

Fig. 3.10. Average computational time of combined constrained and decision feedback detectors in an 8×8 16QAM MIMO system.

Chapter 4

Conclusion

4.1 Summary

The first part of the thesis focuses on the low-complexity optimal detection for MIMO systems. A new detector based on the SD for OFDM/SDMA based wireless systems is proposed. The use of sphere decoding allows optimal detection with computational complexity much less than the naive ML detector in high SNR. Furthermore, it is shown how the CLS detector of [22] is extended to detect non-unitary signals. Next, the hybrid orthogonal STBC and SM system is considered. Such hybrid systems provide a trade off between the rate and the diversity gain. Two new optimal detectors are proposed for these hybrid systems. Our algorithms can also be viewed as a generalization of the conventional SD to handle input matrix symbols. Finally, a new low complexity optimal detector is proposed for a fast fading MIMO OFDM system by taking advantage of the high correlation among neighboring subcarriers in the system. In the proposed algorithm, the subcarriers are partitioned into a number of groups such that the correlation among the subcarriers in each group is high. Within each group, the symbol-detection order is chosen based on the central subcarrier. The same order is then used on other subcarriers in the group to perform the SD.

The second part of the thesis is dedicated to the relaxation of the ML detection

problem in MIMO systems and the development of a family of constrained detectors. Real constrained detectors and decision feedback detectors are proposed for real constellations by forcing the relaxed solution to be real. Modulus constrained subgroup detectors are developed as MIMO detectors for both unitary and non-unitary constellations. A new ordering scheme using these constrained detectors is proposed to achieve a tradeoff between interference suppression and noise enhancement. Moreover, to mitigate the error propagation inherent in decision feedback detectors, a combined constrained and decision feedback detector is introduced. These constrained detectors are suboptimal but they have much less complexity than the SD based optimal detectors in low SNR.

4.2 Future work

Based on the research presented in this thesis, the following work can be carried out in the future:

- In Chapter 2, a modified CLS detector is proposed after the increase of the number of users as a result of non-unitary signals being expressed as a sum of constant modulus signals. This method can be generalized to systems with constant modulus signals that have more users than the number of receive antennas.

- In Chapter 2, a large complexity reduction for the MIMO OFDM system is achieved only when the number of antennas is large. Simulation results show that when the number of antennas is small, for example a (4, 4) system, the complexity reduction is minimal. This is due to the nature of the ordered SD, which provides marginal reduction of computational complexity unless the number of antennas is large. For MIMO OFDM systems with small number of antennas, different algorithms other than the ordered SD must be found to obtain low-complexity optimal detection.

- In Chapter 3, the modulus constrained subgroup method can be extended to MMSE equalizers. This new detector can be derived by solving the prefilter matrix $\mathbf{G}$ in (3.26).

- Also in Chapter 3, the non-convex optimization problem of (3.21) with constraints $\rho_{\min}^2 s_i \leq \mathbf{x}_i^H \mathbf{x}_i$, for $i = 1, \ldots, g$ can be solved by sum of squares method in [68, 69].

References

[1] T. Ojanpera and R. Prasad, "An overview of third-generation wireless personal communications: a European perspective," *IEEE Personal Commun. Mag.*, vol. 5, pp. 59–65, Dec 1998.

[2] A. J. Paulraj, D. A. Gore, R. U. Nabar and H. Bolcskei, "An overview of MIMO communications - a key to gigabit wireless," *Proc. IEEE*, vol. 92, pp. 198–218, Feb 2004.

[3] E. Telatar, "Capacity of multi-antenna Gaussian channels," AT&T-BELL Labs, Tech. Rep., Jun 1995.

[4] G. J. Foschini and M. J. Gans, "On limits of wireless communication in a fading environment when using multiple antennas," *Wireless Personal Commun.*, vol. 6, pp. 311–335, Mar 1998.

[5] G. J. Foschini, "Layered space-time architecture for wireless communication in a fading environment when using multi-element antennas," *Bell Labs Tech. J.,*, vol. 1, pp. 41–59, 1996.

[6] V. Tarokh, N. Seshadri and A. R. Calderbank, "Space-time codes for high data rate wireless communication: Performance analysis and code construction," *IEEE Trans. Inform. Theory*, vol. 44, pp. 744–765, Mar. 1998.

[7] S. M. Alamouti, "A simple transmitter diversity scheme for wireless communication," *IEEE J. Select. Areas Commun.*, vol. 16, pp. 1451–1458, Oct. 1998.

[8] V. Tarokh, H. Jafarkhani, and A. R. Calderbank, "Space-time block codes from orthogonal designs," *IEEE Trans. Inform. Theory*, vol. 45, pp. 1456–1467, July 1999.

[9] ——, "Space-time block coding for wireless communications: Performance results," *IEEE J. Select. Areas Commun.*, vol. 17, pp. 451–460, Mar 1999.

[10] P. W. Wolniansky, G. J. Foschini, G. D. Golden and R. A. Valenzuela, "V-BLAST: an architecture for realizing very high data rates over the rich-scattering wireless channel," *1998 URSI International Symposium on Signals, Systems, and Electronics*, pp. 295–300, Sep 1998.

[11] L. J. Cimini Jr., C. Chuang and N. R. Sollenberger, "Advanced cellular internet service," *IEEE Commun. Mag.*, vol. 36, no. 10, pp. 150–159, Oct 1998.

[12] A. Paulraj, R. Nabar, and D. Gore, *Introduction to space-time wireless communications*. Cambridge University Press, 2003.

[13] G. D. Golden, C. J. Foschini, R. A. Valenzuela and P. W. Wolniansky, "Detection algorithm and initial laboratory results using V-BLAST space-time communication architecture," *Electronics Letters*, vol. 35, no. 1, pp. 14–16, Jan 1999.

[14] S. Anderson, M. Millnert, M. Viberg and B. Wahlberg, "An adaptive array for mobile communication systems," *IEEE Trans. Veh. Technol.*, vol. 40, pp. 230–236, Feb 1991.

[15] S. Talwar, M. Viberg and A. Paulraj, "Blind separation of synchronous co-channel digital signals using an antenna array. I. Algorithms," *IEEE Trans. Signal Processing*, vol. 44, pp. 1184–1197, May 1996.

[16] A. J. Paulraj and C. B. Papadias, "Space-time processing for wireless communications," *IEEE Signal Processing Mag.*, vol. 14, pp. 49–83, Nov 1997.

[17] H. Liu and G. Xu, "Smart antennas in wireless systems: uplink multiuser blind channel and sequence detection," *IEEE Trans. Commun.*, vol. 45, pp. 187–199, Feb 1997.

[18] B. Suard, G. Xu, H. Liu and T. Kailath, "Uplink channel capacity of space-division-multiple-access schemes," *IEEE Trans. Inform. Theory*, vol. 44, pp. 1468–1476, July 1998.

[19] S. B. Weinstein and P. M. Ebert, "Data transmission by frequency division multiplexing using the discrete Fourier transform," *IEEE Trans. Commun.*, vol. 19, pp. 628–634, Oct. 1971.

[20] L. J. Cimini, "Analysis and simulation of a digital mobile channel using orthogonal frequency division multiplexing," *IEEE Trans. Commun.*, vol. COM-33, no. 7, pp. 665–675, July 1985.

[21] J. A. C. Bingham, "Multicarrier modulation for data transmission: An idea whose time has come," *IEEE Commun. Mag.*, vol. 28, pp. 5–14, May 1990.

[22] S. Thoen, L. Deneire, L. Van der Perre, M. Engels and H. De Man, "Constrained least square detector for OFDM/SDMA-based wireless networks," *IEEE Trans. Wireless Commun.*, vol. 2, pp. 129–140, Jan 2003.

[23] J. Jalden and B. Ottersten, "On the complexity of sphere decoding in digital communications," *IEEE Trans. Signal Processing*, vol. 53, no. 4, pp. 1474 – 1484, April 2005.

[24] P. Vandenameele, L. Van der Perre, M. G. E. Engels, B. Gyselinckx and H. J. De Man, "A combined OFDM/SDMA approach," *IEEE J. Select. Areas Commun.*, vol. 18, pp. 2312–2321, Nov 2000.

[25] S. Thoen, L. Van der Perre, M. Engels and H. De Man, "Adaptive loading for OFDM/SDMA-based wireless networks," *IEEE Trans. Commun.*, vol. 50, no. 11, pp. 1798–1809, Nov 2002.

[26] M. Y. Alias, A. K. Samingan, S. Chen and L. Hanzo, "Multiple antenna aided OFDM employing minimum bit error rate multiuser detection," *Electronics Letters*, vol. 39, pp. 1769–1770, Nov 2003.

[27] R. Sood and U. B. Desai, "Minimum probability of error demodulation for multipath OFDM-SDMA systems," *Proc. of WCNC*, vol. 2, pp. 948–953, Mar 2004.

[28] U. Fincke and M. Pohst, "Improved methods for calculating vectors of short length in a lattice, including a complexity analysis," *Mathematics of Computation*, vol. 44, pp. 463–471, Apr 1985.

[29] M. O. Damen, A. Chkeif and J. C. Belfiore, "Lattice codes decoder for space-time codes," *IEEE Commun. Lett.*, vol. 4, pp. 161–163, May 2000.

[30] M. O. Damen, H. El Gamal and G. Caire, "On maximum-likelihood detection and the search for the closest lattice point," *IEEE Trans. Inform. Theory*, vol. 49, no. 10, pp. 2389–2402, Oct 2003.

[31] T. Cui and C. Tellambura, "An efficient generalized sphere decoder for rank-deficient MIMO systems," *IEEE Commun. Lett.*, vol. 9, no. 5, pp. 423–425, May 2005.

[32] ——, "Approximate ML detection for MIMO systems using multistage sphere decoding," *IEEE Signal Processing Lett.*, vol. 12, no. 3, pp. 222–225, Mar 2005.

[33] B. Tarokh and H. R. Sadjadpour, "Construction of OFDM M-QAM sequences with low peak-to-average power ratio," *IEEE Trans. Commun.*, vol. 51, no. 1, pp. 25–28, Jan. 2003.

[34] ETSI TS 101 475 V1.3.1 (2001-12), "Broadband radio access networks (BRAN); HIPERLAN Type 2; Physical (PHY) layer," Dec 2001.

[35] J. Li, K. B. Letaief, R. S. Cheng and Z. Cao, "Multi-stage low complexity maximum likelihood detection for OFDM/SDMA wireless LANs," *Proc. of ICC*, vol. 4, pp. 1152–1156, June 2001.

[36] V. Tarokh, A. Naguib, N. Seshadri and A. R. Calderbank, "Combined array processing and space-time coding," *IEEE Trans. Inform. Theory*, vol. 45, pp. 1121–1128, May 1999.

[37] A. L. F. de Almeida, J. C. M. Mota, W. C. Freitas Jr., F. R. P. Cavalcanti, "Performance of MIMO systems with hybrid of transmit diversity and spatial multiplexing," *Proceedings of Brazilian Telecommunications Symposium*, Oct 2003.

[38] L. Zhao and V. K. Dubey, "Detection schemes for space-time block code and spatial multiplexing combined system," *IEEE Commun. Lett.*, vol. 9, no. 1, pp. 49–51, Jan 2005.

[39] ——, "Transmit diversity and combining scheme for spatial multiplexing over correlated channels," *Proc. of VTC*, vol. 1, pp. 380–383, May 2004.

[40] E. G. Larsson and P. Stoica, *Space-time block coding for wireless communications*. Cambridge University Press, 2003.

[41] W. Yan, S. Sun, and Z. Lei, "a low complexity VBLAST OFDM detection algorithm for wireless LAN systems," *IEEE Commun. Lett.*, vol. 8, pp. 374–376, Jun 2004.

[42] J. Foschini, G. Golden, R. Valenzuela, and P. Wolniansky, "Simplified processing for high spectral efficiency wireless communication employing multi-element arrays," *IEEE J. Select. Areas Commun.*, vol. 17, pp. 1841–1352, Nov 1999.

[43] J. Medbo, H. Hallenberg, and J.-E. Berg, "Propagation characteristics at 5 GHz in typical radio-LAN scenarios," *Proc. of VTC*, vol. 1, pp. 185–189, May 1999.

[44] A. Yener, R. D. Yates, and S. Ulukus, "CDMA multiuser detection: a nonlinear programming approach," *IEEE Trans. Commun.*, vol. 50, no. 6, pp. 1016 – 1024, June 2002.

[45] W.-J. Choi, R. Negi, and J. M. Cioffi, "Combined ML and DFE decoding for the V-BLAST system," in *Proc. of ICC*, vol. 3, June 2000, pp. 1243 – 1248.

[46] G. Ginis and J. M. Cioffi, "On the relation between V-BLAST and the GDFE," *IEEE Commun. Lett.*, vol. 5, no. 9, pp. 364 – 366, Sept. 2001.

[47] A. Benjebbour, H. Murata, and S. Yoshida, "Comparison of ordered successive receivers for space-time transmission," in *Proc. of VTC*, vol. 4, Oct. 2001, pp. 2053 – 2057.

[48] E. Viterbo and J. Boutros, "A universal lattice code decoder for fading channels," *IEEE Trans. Inform. Theory*, vol. 45, pp. 1639–1642, Jul 1997.

[49] W.-K. Ma, T. Davidson, K. M. Wong, Z.-Q. Luo, and P.-C. Ching, "Quasi-maximum-likelihood multiuser detection using semi-definite relaxation with application to synchronous CDMA," *IEEE Trans. Signal Processing*, vol. 50, no. 4, pp. 912 – 922, April 2002.

[50] W.-K. Ma, P.-C. Ching, and Z. Ding, "Semidefinite relaxation based multiuser detection for M-ary PSK multiuser systems," *IEEE Trans. Signal Processing*, vol. 52, no. 10, pp. 2862 – 2872, Oct. 2004.

[51] P. H. Tan and L. Rasmussen, "The application of semidefinite programming for detection in CDMA," *IEEE J. Select. Areas Commun.*, vol. 19, no. 8, pp. 1442 – 1449, Aug. 2001.

[52] A. Wiesel, Y. C. Eldar, and S. Shamai, "Semidefinite relaxation for detection of 16-QAM signaling in MIMO channels," *IEEE Signal Processing Lett.*, vol. 12, pp. 653–656, Sep 2005.

[53] N. D. Sidiropoulos and Z.-Q. Luo, "A semidefinite relaxation approach to MIMO detection for high-order QAM constellations," *IEEE Signal Processing Lett.*, vol. 13, pp. 525–528, Sep 2006.

[54] S. Haykin, *Adaptive Filter Theory*, 4th ed. Prentice Hall, Sept. 2001.

[55] P. H. Tan and L. Rasmussen, "Multiuser detection in CDMA - a comparison of relaxations, exact, and heuristic search methods," *IEEE Trans. Wireless Commun.*, vol. 3, no. 5, pp. 1802–1809, Sept. 2004.

[56] W. H. Press, S. A. Teukolsky, W. T. Vetterling and B. P. Flannery, *Numerical recipes in C - the art of scientific computing*, 2nd ed. Cambridge University Press, 1992.

[57] G. E. Forsythe and G. H. Golub, "On the stationary values of a second degree polynomial on the unit sphere," *J. Soc. Indust. Appl. Math,*, vol. 13, no. 1050-1068, 1965.

[58] S. Boyd and L. Vandenberghe, *Convex Optimization*. Cambridge University Press, March 2004.

[59] N. Z. Shor, *Minimization methods for non-differentiable functions*. Springer-Verlag, 1985.

[60] D. Chase, "Class of algorithms for decoding block codes with channel measurement information," *IEEE Trans. Inform. Theory*, vol. 18, no. 1, pp. 170 – 182, Jan. 1972.

[61] D. J. Love, S. Hosur, A. Batra, and R. Heath, "CDMA multiuser detection: a nonlinear programming approach," *IEEE Trans. Wireless Commun.*, vol. 4, no. 5, pp. 2035 – 2039, Sept. 2005.

[62] D. W. Waters and J. R. Barry, "The chase family of detection algorithms for multiple-input multiple-output channels," in *Proc. of GLOBECOM*, vol. 4, Nov. 2004, pp. 2635 – 2639.

[63] T. Cui and C. Tellambura, "Generalized feedback detection for MIMO systems," in *Proc. of GLOBECOM*, 2005.

[64] A. Papoulis and S. Pillai, *Probability, Random Variables and Stochastic Processes*. McGraw-Hill Education, Dec. 2001.

[65] S. Loyka and F. Gagnon, "Performance analysis of the V-BLAST algorithm: An analytical approach," *IEEE Trans. Wireless Commun.*, vol. 3, no. 4, pp. 1326–1337, July 2004.

[66] Y. Jiang, X. Zheng, and J. Li, "Asymptotic performance analysis of V-BLAST," in *Proc. of GLOBECOM*, Nov 2005.

[67] R. Fischer and C. Windpassinger, "Real versus complex-valued equalisation in V-BLAST systems," *Electronics Letters*, vol. 39, no. 5, 6, pp. 470 – 471, March 2003.

[68] T. Cui, T. Ho, and C. Tellambura, "Polynomial moment relaxation for MIMO detection," *Proc. of ICC*, vol. 7, pp. 3129–3134, Jun 2006.

[69] J. B. Lasserre, "Global optimization with polynomials and the problem," *SIAM J. Optim.*, vol. 11, no. 3, pp. 796–817, 2001.